Higher-Order Turbulence Closure and Its Impact on Climate Simulations in the Community Atmosphere Model

PETER A. BOGENSCHUTZ, ANDREW GETTELMAN, AND HUGH MORRISON

National Center for Atmospheric Research, Boulder, Colorado*

VINCENT E. LARSON

University of Wisconsin–Milwaukee, Milwaukee, Wisconsin

CHERYL CRAIG

National Center for Atmospheric Research, Boulder, Colorado*

DAVID P. SCHANEN

University of Wisconsin–Milwaukee, Milwaukee, Wisconsin

(Manuscript received 30 January 2013, in final form 31 May 2013)

ABSTRACT

This paper describes climate simulations of the Community Atmosphere Model, version 5 (CAM5), coupled with a higher-order turbulence closure known as Cloud Layers Unified by Binormals (CLUBB). CLUBB is a unified parameterization of the planetary boundary layer (PBL) and shallow convection that is centered around a trivariate probability density function (PDF) and replaces the conventional PBL, shallow convection, and cloud macrophysics schemes in CAM5. CAM–CLUBB improves many aspects of the base state climate compared to CAM5. Chief among them is the transition of stratocumulus to trade wind cumulus regions in the subtropical oceans. In these regions, CAM–CLUBB provides a much more gradual transition that is in better agreement with observational analysis compared to CAM5, which is too abrupt. The improvement seen in CAM–CLUBB can be largely attributed to the gradual evolution of the simulated turbulence, which is in part a result of the unified nature of the parameterization, and to the general improved representation of shallow cumulus clouds compared to CAM5. In addition, there are large differences in the representation and structure of marine boundary layer clouds between CAM–CLUBB and CAM5. CAM–CLUBB is also shown to be more robust, in terms of boundary layer clouds, to changes in vertical resolution for global simulations in a preliminary test.

1. Introduction

Despite advances made in computational power over the last several decades, atmospheric general circulation models (GCMs) often still employ highly parameterized physics. While global cloud-resolving models (Tomita et al. 2005; Miura et al. 2005) and so-called superparameterized GCMs (Khairoutdinov et al. 2005) are emerging, it appears that conventionally parameterized GCMs will remain as the computational feasible route in performing century-long global climate simulations for quite some time.

Most GCMs still use separate schemes for physical processes, such as the planetary boundary layer (PBL), shallow and deep cumulus convection, and stratiform clouds. However, in nature these are often not discrete regimes and this has driven a search for so-called unified parameterizations (Lappen and Randall 2001). One important example is the regions of stratocumulus to cumulus transition over subtropical oceans, which GCMs often simulate poorly since it is not clear if the PBL or

*The National Center for Atmospheric Research is sponsored by the National Science Foundation.

Corresponding author address: Peter A. Bogenschutz, P.O. Box 3000, Boulder, CO 80307.
E-mail: bogensch@ucar.edu

DOI: 10.1175/JCLI-D-13-00075.1

shallow convection scheme should parameterize this cloud type (cumulus under stratocumulus). Indeed, recent studies (Kay et al. 2012; Teixeira et al. 2011) show that many GCMs, such as the Community Atmosphere Model, version 5 (CAM5), struggle to simulate the stratocumulus to cumulus transition. In addition, shallow cumulus clouds are often thought to be extended moist plumes of boundary layer turbulence and the tight coupling between PBL eddies and shallow convection makes it difficult to separate the two processes (Arakawa 2004).

Over the last decade, development of unified parameterizations has been an active area of research. Two such methods have been proposed for GCM applications. The first is known as the eddy diffusion mass flux (EDMF) approach (Siebesma et al. 2007; Pergaud et al. 2009), which seeks to unify PBL and shallow convective processes by the marriage of traditionally used diffusion schemes in the PBL and the commonly used mass flux approach to parameterize convection. The second method is known as higher-order turbulence closure (HOC). HOC methods, which seek to predict the unclosed turbulent moments that appear in the governing equations, have been used for decades to simulate stratus and shallow cumulus clouds (e.g., Moeng and Randall 1984; Bougeault 1981). However, recent work (Golaz et al. 2002) has sought to modernize HOC by linking the schemes to a trivariate double-Gaussian PDF probability density function (PDF), which allows for a more consistent closure treatment for unclosed higher-order turbulent moments as well as a unified cloud scheme for boundary layer clouds of all types.

While both EDMF and modernized HOC schemes have documented much success in simulating Global Energy and Water Cycle Experiment (GEWEX) Cloud System Study (GCSS) boundary layer cases in single-column models (SCMs; e.g., Pergaud et al. 2009; Golaz et al. 2002; Cheng and Xu 2008), their testing and applications into GCMs has thus far been virtually nonexistent. One noteworthy exception is the work of Cheng and Xu (2011), which implemented a HOC scheme into the embedded cloud-resolving model of a superparameterized GCM with improved simulation of boundary layer clouds. However, the application of these unified schemes into conventionally parameterized GCMs is just now emerging. Guo et al. (2010) implemented a HOC scheme, known as Cloud Layers Unified by Binormals (CLUBB; Golaz et al. 2002), into the Geophysical Fluid Dynamic Laboratory (GFDL) Atmosphere Model, version 3 (AM3), and showed that in the single-column framework boundary layer clouds and aerosol effects could be realistically simulated. Bogenschutz et al. (2012) showed that CLUBB implemented into CAM5 could achieve more realistic shallow convective clouds and transitional type (i.e., cumulus under stratocumulus) of boundary layer clouds when compared to standard CAM5 physics in single-column simulations. In addition, they showed that sensitivity to time step and vertical resolution was reduced with the addition of CLUBB.

This paper will build on the single-column results of Bogenschutz et al. (2012) and present global climate simulations of a HOC scheme (CLUBB) coupled with CAM5. The coupling of CAM5 with CLUBB is referred to as CAM–CLUBB. Bogenschutz et al. (2012) list several of the conceptual advantages of CAM–CLUBB over CAM5. In the CAM–CLUBB configuration, the conventional PBL, shallow convection, and cloud macrophysics parameterizations are all replaced by CLUBB, which is responsible for calculating tendencies from these processes with one equation set. The unified nature of CLUBB is the most significant conceptual advantage over traditional CAM5 physics because 1) inconsistencies from calling many different parameterizations (i.e., separate shallow convection and PBL schemes) that may or may not be compatible with one another are avoided, 2) there are no trigger functions to determine which scheme to call for rather ambiguous regimes such as cumulus under stratocumulus, and 3) a unified parameterization of shallow convection and PBL clouds can drive a single microphysics scheme. In CAM5 the deep convection and shallow convection schemes contain their own simplified single-moment treatments of microphysics, while stratiform microphysics is handled by the double-moment Morrison–Gettelman (MG) scheme (Morrison and Gettelman 2008). Therefore, by driving the MG scheme for both PBL and shallow convective cloud using CLUBB, this can lead to a more consistent treatment of microphysics processes as well as a more consistent treatment of cloud–aerosol interactions. However, the CAM–CLUBB experiments presented in this paper still include a traditional deep convective parameterization.

The paper is organized as follows: Section 2 will describe the physics differences between CAM5 and CAM–CLUBB, while section 3 will discuss the simulations performed in this paper. Section 4 will present climate simulation results from CAM5 and CAM–CLUBB, including an analysis of boundary layer clouds and sensitivity to changes in vertical resolution. Finally, section 5 will conclude with a discussion and remarks for future work.

2. Model descriptions

CAM5 (Neale et al. 2010) is used as the control model in this study. CAM5 represents nearly a complete overhaul in physical parameterization options from CAM4, with the exception of the deep convection Zhang–McFarlane

TABLE 1. Summary of physics used in CAM5 and CAM–CLUBB.

Physics	CAM5	CAM–CLUBB
Deep convection	Zhang and McFarlane 1995	Zhang and McFarlane 1995
Boundary layer	Bretherton and Park 2009	CLUBB
Shallow convection	Park and Bretherton 2009	CLUBB
Cloud macrophysics	Park (Neale et al. 2010)	CLUBB
Cloud microphysics	Morrison and Gettelman 2008	Morrison and Gettelman 2008
Radiation	Rapid Radiative Transfer Model for GCMs (RRTMG); Iacono et al. 2008	RRTMG; Iacono et al. 2008
Aerosols	Liu et al. 2012	Liu et al. 2012

(ZM) scheme (Zhang and McFarlane 1995; Neale et al. 2008; Richter and Rasch 2008). The boundary layer scheme is based on downgradient diffusion of moist conserved variables [University of Washington moist turbulence (UWMT); Bretherton and Park 2009], the shallow convection scheme in CAM5 is from Park and Bretherton (2009) [University of Washington shallow convection (UWSC)], and cloud macrophysics is computed according to the Park macrophysics as described in Neale et al. (2010). Morrison and Gettelman (2008) two-moment stratiform microphysics for both liquid and ice is used in CAM5, as described in Gettelman et al. (2010). Aerosols are predicted according to Liu et al. (2012) and linked to the microphysics through the parameterization of liquid and ice activation of cloud drops and crystals on aerosols (Gettelman et al. 2010).

The CAM–CLUBB configuration is described in detail in Bogenschutz et al. (2012); therefore, only a brief overview is presented here. CAM–CLUBB differs from CAM5 in terms of the physics options (Table 1). In CAM–CLUBB, the UWMT, UWSC, and Park macrophysics are replaced by CLUBB. Therefore, CLUBB is responsible for calculating tendencies resulting from boundary layer mixing, shallow convection, and cloud macrophysics in one parameterization call that is based on one equation set. The current version of CLUBB predicts $\overline{\theta_l}$ (liquid water potential temperature), $\overline{q_t}$ (total water mixing ratio), $\overline{u}$ (zonal wind), $\overline{v}$ (meridional wind), $\overline{u'^2}$, $\overline{v'^2}$, $\overline{\theta_l'^2}$, $\overline{q_t'^2}$, $\overline{\theta_l' q_t'}$, $\overline{w' q_t'}$, $\overline{w' \theta_l'}$, $\overline{w'^2}$, and $\overline{w'^3}$ (where w is vertical velocity). Here, the overbar denotes grid-mean quantities and the prime denotes perturbations from the mean.

In addition to providing temperature, moisture, and momentum tendencies resulting from boundary layer turbulence and convection, CLUBB also computes the warm cloud fraction C and cloud liquid water mixing ratio from the assumed joint PDF. These are important macrophysical cloud quantities that are needed for the computation of radiative, microphysical, and aerosol processes. In addition, a subgrid-scale (SGS) vertical velocity is needed for aerosol activation because droplet activation depends on local rather than grid-scale vertical velocity (Ghan et al. 1997). In CAM5 this is done by deriving the SGS vertical velocity w' from the diagnosed turbulent kinetic energy (TKE) computed in the UWMT scheme. In CAM–CLUBB, w' is derived from the predicted value of $\overline{w'^2}$.

The version of CAM–CLUBB presented in this paper differs from the version presented in Bogenschutz et al. (2012), mostly in terms of the modified parameters used to achieve realistic cloud radiative forcing (CRF). These parameter settings are described in appendix A. In addition, one physical upgrade was made to the CAM–CLUBB configuration since the Bogenschutz et al. (2012) version. Namely, the Morrison and Gettelman (2008) microphysics scheme assumes that the PDF of in-cloud water follows a gamma distribution, which includes the assumption of a constant cloud water variance. Since the CLUBB parameterization outputs cloud water variance $\overline{q_c'^2}$; this term is now passed from CLUBB to the MG microphysics scheme.

For the warm cloud boundary layer cases presented in Bogenschutz et al. (2012), ice processes were never considered or discussed. Because CLUBB is currently a warm cloud parameterization, ice cloud fraction is closed using the current relative humidity based scheme as described by Gettelman et al. (2010). We feed the microphysics and radiation the cloud fraction (i.e., CLUBB or ice cloud fraction) associated with the larger mixing ratio between liquid or ice. Ice mass and number mixing ratios are transported in CLUBB via a simple eddy diffusion scheme based on eddy diffusivity as a function of CLUBB's turbulence length scale and turbulent kinetic energy. Currently, CAM chemistry constituents are also transported by the same scheme. All aerosol constituents and cloud droplet number concentration, however, are transported by the large-scale advection in CAM.

3. Model simulations

Using present-day emissions, both CAM5 and CAM–CLUBB are integrated for 5 yr at 1° horizontal resolution

using the CAM5 finite volume dynamical core (Neale et al. 2010). These CAM simulations rely on prescribed sea surface temperatures (SSTs). Fully coupled CAM–CLUBB simulations in the Community Earth System Model (CESM) will be left to future work. However, initial coupled experiments of CAM–CLUBB indicate that short climate simulations are stable. To achieve a better comparison with satellite observations, the Coupled Model Intercomparison Project (CMIP) Observing Satellite Package (COSP; Kay et al. 2012) is turned on for the last 2 yr of each CAM5 and CAM–CLUBB simulations. CAM5 and CAM–CLUBB are also run with 60 vertical levels to elucidate the sensitivity of physics packages to vertical resolution (the standard configuration of CAM5 has 30 vertical levels).

CAM–CLUBB simulations have a 20% increase in computational cost over CAM5 simulations. We do not feel this increase imposes undue burdens to GCM modelers. For a 1-month simulation on the National Center for Atmospheric Research (NCAR) Yellowstone supercomputer (IBM iDataPlex DX360M4) at 2° resolution and using the finite volume dynamical core, CAM5 completed integration in 387 s and CAM–CLUBB completed integration in 465 s. Both of these simulations utilized 256 processors and a 30-min CAM time step. These numbers from CAM–CLUBB represent the standard configuration, in which the CLUBB time step is 5 min. Computational cost of CAM–CLUBB can be reduced by lengthening the CLUBB time step. Preliminary results show that using a CLUBB time step of 10 min produces comparable results to those presented in this paper, with nearly equal computational performance compared to CAM5.

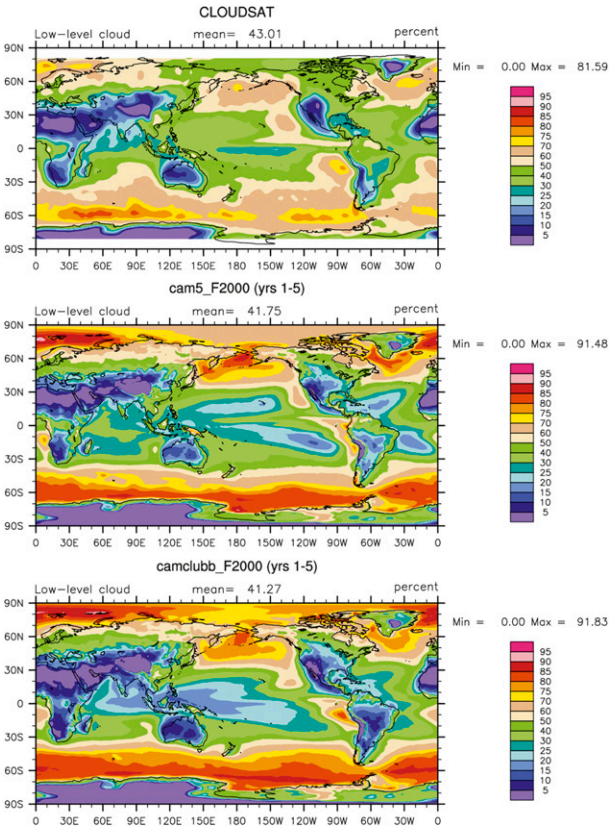

FIG. 1. Low cloud amounts averaged over the 5-yr simulation of (middle) CAM5 and (bottom) CAM–CLUBB and for (top) observations (*CloudSat–CALIPSO*).

4. Results

The first subsection of the results will focus on the mean state of the 1° simulations, while section 4b will present a detailed analysis of boundary layer clouds for both CAM5 and CAM–CLUBB. Finally, section 4c will briefly present sensitivity to vertical resolution in CAM5 and CAM–CLUBB. For the analysis in this paper, the first 2 months of the simulation are thrown out and the simulations are run out to the third month of the sixth year and we refer to this as our 5-yr average.

a. Mean state climate

Since one of the main purposes of implementing CLUBB into CAM was to better represent boundary layer processes, we will first focus on metrics relating to boundary layer clouds. Figure 1 displays the integrated low cloud amount, where the top panel indicates *CloudSat–Cloud–Aerosol Lidar and Infrared Pathfinder Satellite Observations* (*CALIPSO*) observations while the middle and bottom panels are the simulated results for CAM5 and CAM–CLUBB, respectively. Figure 2 presents the bias plots for both configurations, computed with respect to *CloudSat–CALIPSO* observations. The bias plots for CAM5 clearly show the abrupt transition from stratocumulus (Sc) to cumulus (Cu) found off the western coasts of all the major continents, also noted by Kay et al. (2012). To a degree, CAM–CLUBB also appears to suffer from this bias; however, it is ameliorated as all Sc–Cu transition areas appear to be represented more smoothly and in better agreement with observations. This is consistent with the SCM study (Bogenschutz et al. 2012) that found much more realistic simulation of Cu rising into Sc. CAM5, however, tends to simulate a more or less purely Cu regime for these transition zones. The improved simulation is due to gradual turbulence evolution owed in part to the unified nature of CLUBB in its treatment of boundary layer clouds (discussed in further detail in section 4b), whereas in CAM5 the shallow convection scheme tends to activate and take over too quickly (Medeiros et al. 2012).

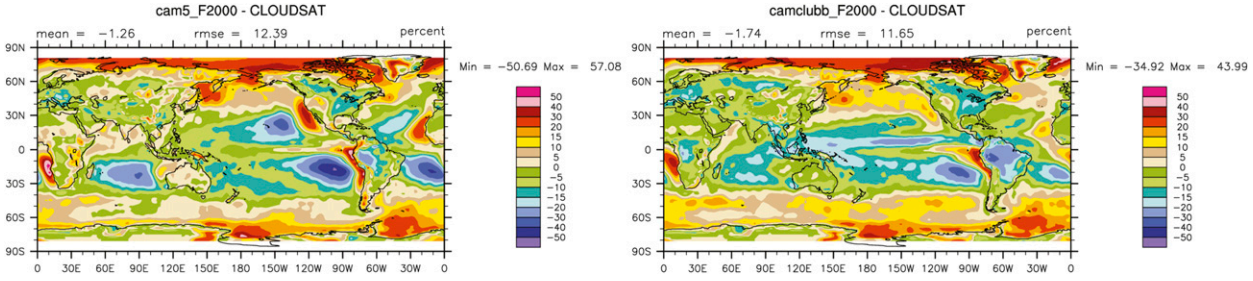

FIG. 2. Differences between 5-yr model simulation for (left) CAM5 and (right) CAM–CLUBB and observations (*CloudSat–CALIPSO*) for the low cloud amount.

Shortwave cloud forcing (SWCF) is one of the most important metrics to examine for improving the representation of boundary layer clouds. The observations and simulated SWCF can be found in Fig. 3, whereas the model biases are presented in Fig. 4. Both CAM5 and CAM–CLUBB qualitatively capture the main features and patterns of the observed SWCF as indicated by the Clouds and the Earth's Radiant Energy System (CERES) Energy Balance and Filled (EBAF) product. However, CAM–CLUBB does contain a number of notable improvements, including RMSE, which is nearly $2\,\mathrm{W\,m^{-2}}$ lower than CAM5. The first regional improvement is over the Southern Ocean, where boundary layer clouds of both cumulus and stratiform are common. Reduced biases (Fig. 4), relative to CAM5, are also found in most of the Sc–Cu transitional regions in the tropical and subtropical oceans. In these regions, CAM5 clouds become too dim too close to the coastlines, whereas CAM–CLUBB provides a more gradual and realistic transition. The top-right panel of Fig. 5 displays the zonal averages of CAM5 and CAM–CLUBB for SWCF with CERES-EBAF observations. In this figure, the improvements in the Southern Ocean and tropics for CAM–CLUBB become very apparent.

A notable bias unique to CAM–CLUBB can be found in the California coastal Sc, where the clouds are too dim relative to observations and CAM5. This is not an issue for the more offshore Sc, which is actually too bright. While it is possible to retain these coastal Sc clouds in CAM–CLUBB by modifying CLUBB's tunable parameters, it is at the expense of representing trade wind cumulus and global CRF. This raises a unique predicament when implementing unified physical parameterizations into global models. Whereas these unified parameterizations are very physically appealing, biases cannot simply be tuned away as easily in GCMs that use modular physics since the simulated atmospheric phenomena are all connected by the same equation set. Therefore, more physical solutions are required (as opposed to tuning) with these unified parameterizations to achieve realistic regional distributions of CRF. For instance, the variable cloud water variance passed from CLUBB to MG improves the regional CRF. Future work will involve a tighter coupling between CLUBB and MG that may improve coastal Sc by integrating over the PDF and introducing subcolumns for microphysical process rates (Pincus et al. 2006).

Climatology of the oceanic liquid water path (LWP) can be found in Fig. 6. In this figure it is obvious that both CAM5 and CAM–CLUBB contain much less LWP than observations; however, both CAM models contain reasonable patterns. CAM–CLUBB shows some regional

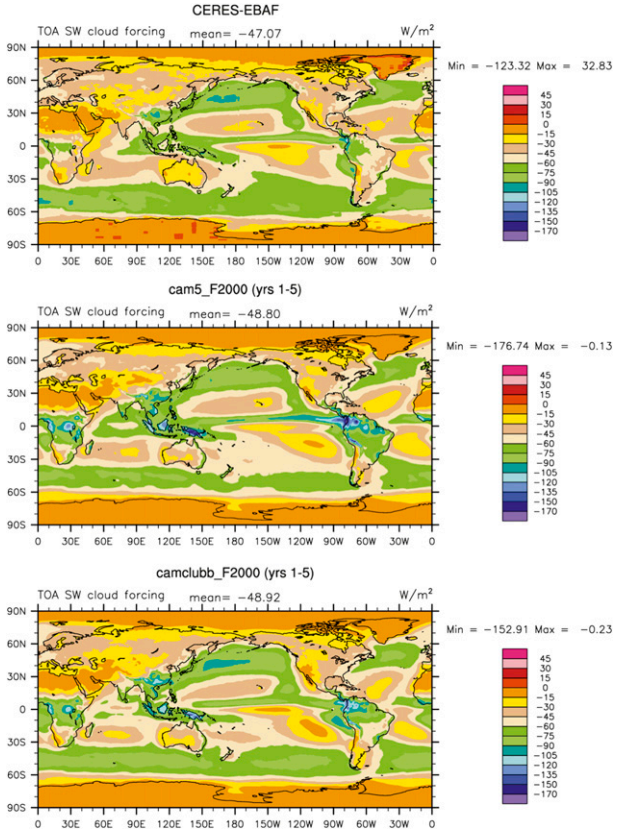

FIG. 3. As in Fig. 1, but for SWCF with (top) CERES-EBAF serving as the observational analysis.

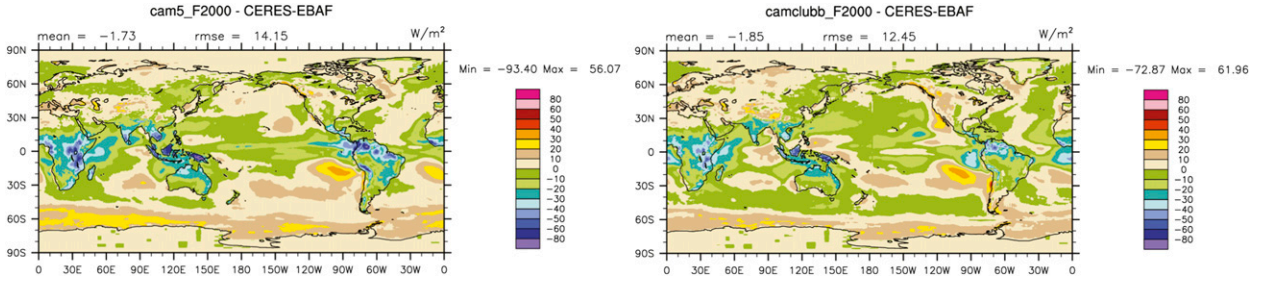

FIG. 4. Differences between 5-yr model simulation for (left) CAM5 and (right) CAM–CLUBB and observations CERES-EBAF for SWCF.

improvements, such as higher values of LWP in the Northern and Southern Hemispheric storm tracks in addition to more liquid in the stratocumulus and stratocumulus to cumulus transition regions. However, deep convective regions (e.g., the ITCZ) and some shallow convective regions in CAM–CLUBB do contain less liquid water than CAM5.

Although the goal of implementing CLUBB into CAM was not to improve representation of high-level clouds, it is still important to make sure that longwave cloud forcing (LWCF), dominated by high clouds, is not negatively affected by the addition of CLUBB. Figure 5 displays the zonal averages of LWCF, SWCF, midlevel cloud amount, and high-level cloud amount. The underprediction of LWCF by CAM5 is a persistent bias in the model resulting from poor representation of thin high-level stratiform clouds. CAM–CLUBB neither helps nor significantly hurts this LWCF bias as the pattern and distribution is realistic and comparable to that of CAM5 and observations (not shown). In addition, midlevel cloud and high-level cloud is very similar in representation for CAM5 and CAM–CLUBB. Regional biases follow those presented in Kay et al. (2012).

For the surface precipitation rate, CAM–CLUBB has lower RMSE when compared to CAM5 (Table 2). Climatology of the total precipitation rates for observations

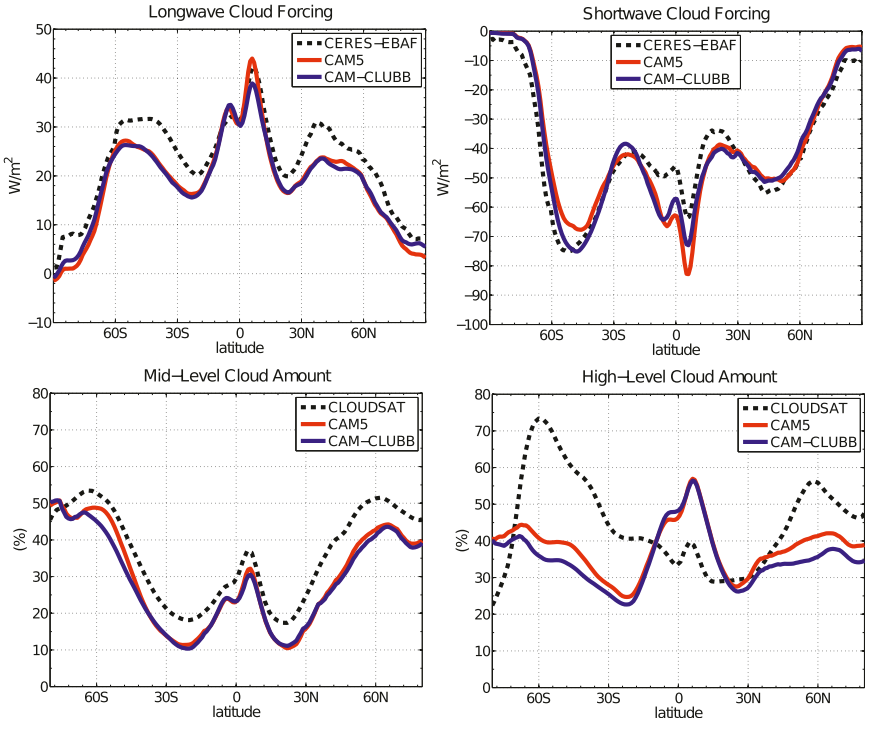

FIG. 5. Zonal means of the (top left) LWCF, (top right) SWCF, (bottom left) midlevel cloud amount, and (bottom right) high-level cloud amount. Red and blue curves denote the 5-yr zonal averages for CAM5 and CAM–CLUBB, respectively. Black dashed curves denote observation.

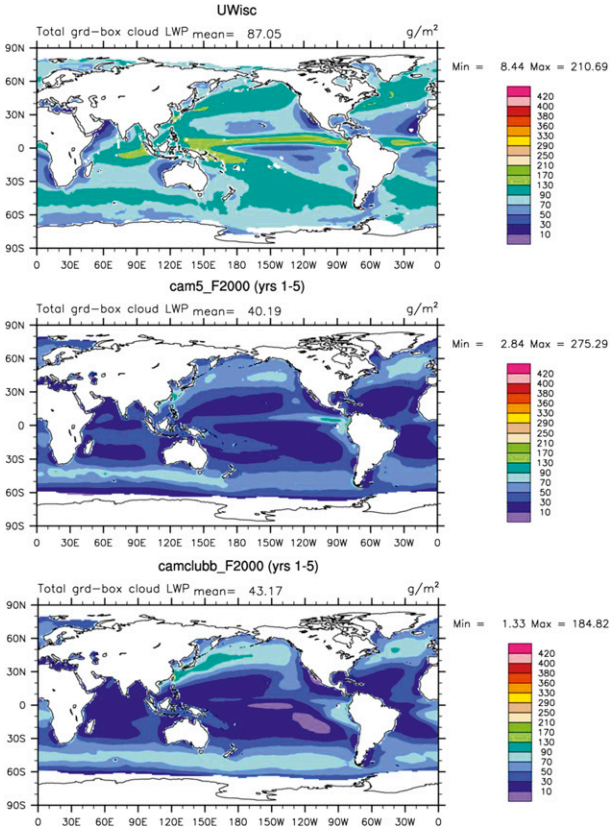

FIG. 6. As in Fig. 1, but for LWP with University of Wisconsin serving as the observational analysis.

and each simulation can be found in Fig. 7, whereas zonal averages are displayed in Fig. 8. An examination of the zonal averages and regional distributions show that most of the bias improvement for CAM–CLUBB originates along the maritime deep convective regions of the ITCZ. This result is somewhat surprising given the fact that the ZM deep convection scheme is still just as active in climatically favorable regions for deep convection in CAM–CLUBB. For these grid columns CLUBB only contributes tendencies in the lower troposphere while the ZM scheme takes over in the middle and upper levels.

A more detailed examination of precipitation is performed by looking at zonal averages of the partitioning of precipitation types (i.e., deep convective, shallow convective, and large-scale precipitation types; Fig. 8). Recall that in CAM–CLUBB the Park and Bretherton (2009) shallow convection scheme is turned off and therefore all shallow convective precipitation is zero everywhere and the stratiform MG microphysics scheme is responsible for shallow convective precipitation. While the contribution from the ZM scheme is greater for CAM5 than CAM–CLUBB in the ITCZ, it does not account for the nearly 1.5 mm day^{-1} total precipitation difference. The majority of the difference comes from the shallow convection scheme in CAM5. In a sense, the improved representation of precipitation in CAM–CLUBB compared to CAM5 is a result of the absence of the shallow convective scheme which appears to be responsible for the large biases in CAM5.

Finally, Fig. 9 shows a Taylor diagram (Taylor 2001) comparing CAM5 and CAM–CLUBB for several climatically important variables. Taylor diagrams provide a convenient and compact display to compare two models against observations, with a better model residing closer to the reference (REF) point. CAM–CLUBB is not very dissimilar from CAM5 for many variables on this figure, such as LWCF, temperature, and zonal winds. However, any differences between the two configurations are generally in favor of CAM–CLUBB. These improvements can be seen in land rainfall, ocean rainfall, sea level pressure, and Pacific Ocean stress. All of these have better variability when compared to observations. In addition, root-mean-square error scores for several important climatic atmosphere variables can be found in Table 2. Many improvements (and some degradations) are found in the mean state climate for CAM–CLUBB. Global averages, including top-of-atmosphere (TOA) energy imbalance, can be found in Table 3.

The fact that CAM–CLUBB appears to improve the general low cloud climatology in addition to not degrading (and, in some cases, improving) the metrics of the base state climate bodes well for this model configuration. Although CAM–CLUBB goes a long way in ameliorating biases found along the stratocumulus to cumulus transition zones (Figs. 1–4), the overall bias patterns exhibited by CAM–CLUBB for low cloud amounts and SWCF are very similar to those of CAM5. One could easily assume that even though we have replaced most of the cloud forming physics with new unified physics that we are simply achieving roughly the same clouds that CAM5 simulates. However, the coming sections will focus on an assessment of the Sc–Cu transition and the cloud structure of these boundary layer clouds as simulated by CAM–CLUBB to show that this is not true.

b. Boundary layer clouds in CAM5 and CAM–CLUBB

In the previous section, CAM–CLUBB demonstrated more realistic subtropical stratocumulus to cumulus transition characteristics through annually averaged two-dimensional analysis of low cloud amounts and SWCF. Here we take a closer look by examining cross sections depicting the Sc–Cu transition as well as the vertical structure and temperature profiles of boundary layer clouds in the two configurations of CAM.

TABLE 2. RMSE summary for CAM5 and CAM–CLUBB for the 5-yr simulations.

Variable	Observation source	Units	CAM5	CAM–CLUBB
Low-level cloud amount	*CloudSat*	%	12.39	11.65
Medium-level cloud amount	*CloudSat*	%	8.77	9.24
High-level cloud amount	*CloudSat*	%	9.46	9.18
Shortwave cloud forcing	CERES-EBAF	$W m^{-2}$	14.15	12.45
Longwave cloud forcing	CERES-EBAF	$W m^{-2}$	6.90	7.61
Global precipitation rate	Global Precipitation Climatology Project (GPCP)	$mm day^{-1}$	1.16	0.97
Land precipitation rate	Climate Prediction Center (CPC) Merged Analysis of Precipitation (CMAP)	$mm day^{-1}$	1.32	1.04
Ocean tropical precipitation rate	GPCP	$mm day^{-1}$	1.43	1.16
Global precipitable water	National Aeronautics and Space Administration (NASA) Water Vapor Project (NVAP)	mm	2.15	1.91
Tropical precipitable water	NVAP	mm	2.61	2.31
Global 2-m air temperature	Legates	K	3.34	3.34
Land 2-m air temperature	Willmott	K	2.70	2.57
850-hPa temperature	AIRS	K	1.15	1.22
200-hPa temperature	AIRS	K	4.15	3.18
Sea level pressure	National Centers for Environmental Prediction (NCEP)	hPa	3.28	3.72
TOA albedo	CERES-EBAF	—	0.05	0.05
Liquid water path (ocean)	University of Wisconsin	$g m^{-2}$	52.44	52.95
Surface latent heat flux	Woods Hole Oceanographic Institution	$W m^{-2}$	30.53	26.59
Surface sensible heat flux	Large and Yeager	$W m^{-2}$	9.84	11.67
Surface water flux	Large and Yeager	$mm day^{-1}$	0.79	0.75

First, we focus our attention on the five main subtropical Sc–Cu transition regions, with the locations of five cross sections displayed in Fig. 10. Observational guidance is provided from *CALIPSO*, *CloudSat*, and Moderate Resolution Imaging Spectroradiometer (MODIS) in a merged product called C3M (Kato et al. 2010). Figure 11 displays the cross sections of cloud fraction for the five cross sections, averaged over the 5-yr simulations, for the two CAM configurations and C3M. For many of the regions, C3M generally shows a gradual reduction of cloud cover along with a rising cloud-top height and thickening cloud depth moving downstream off the coasts. However, CAM5 tends to abruptly reduce cloud amount outside of the coastal stratocumulus regions. In addition, CAM5 fails to simulate the higher cloud-top height farther from the coast as C3M suggests. This is most prevalent in the South American and Southern African cross sections. The transitions for CAM–CLUBB depict a much different picture. While cloud amounts are generally low when compared to C3M, the qualitative aspects of the transition are better captured for all regions: most notably the rising of cloud top as it moves offshore and the placement of the maximum cloudiness, which generally occurs somewhat offshore in C3M. CAM5 generally simulates maximum cloud amount right along the coast (e.g., in the South American region).

The same presentation, but for the gridbox averaged cloud liquid mixing ratio, can be found in Fig. 12. In general, the same arguments made for cloud fraction also apply here. It should be noted that for most of the trade cumulus regions (the left side of each plot) both configurations of CAM underestimate the amount of liquid water. However, both configurations of CAM overestimate liquid water in the stratocumulus regions. An underrepresentation of the liquid water path in CAM5 relative to satellite observations remains a bias in CAM–CLUBB (as shown in Fig. 6). However, in CAM–CLUBB the trade cumulus regions do appear to contain more liquid water than CAM5 and in better agreement with C3M. In addition, the overall characteristics of the gradual transition demonstrated by C3M are more realistically captured for CAM–CLUBB, albeit the transition generally still occurs too abruptly in most regions for this model configuration. The exception is the California region, where CAM–CLUBB uniformly overpredicts liquid water across the entire transition region.

Cross sections of some turbulence statistics from the South America cross section can be found in Fig. 13 for CAM–CLUBB. Here the third moment of vertical velocity $\overline{w'^3}$ and buoyancy flux $\overline{w'\theta_v'}$ are displayed to demonstrate CAM–CLUBB's ability to realistically simulate the transition from stratocumulus to cumulus. Although climatological observations of these quantities are not readily available, the characteristics demonstrated by $\overline{w'^3}$ and $\overline{w'\theta_v'}$ are what we would expect based on large-eddy simulation (LES) guidance of idealized boundary layer cloud cases (Golaz et al. 2005).

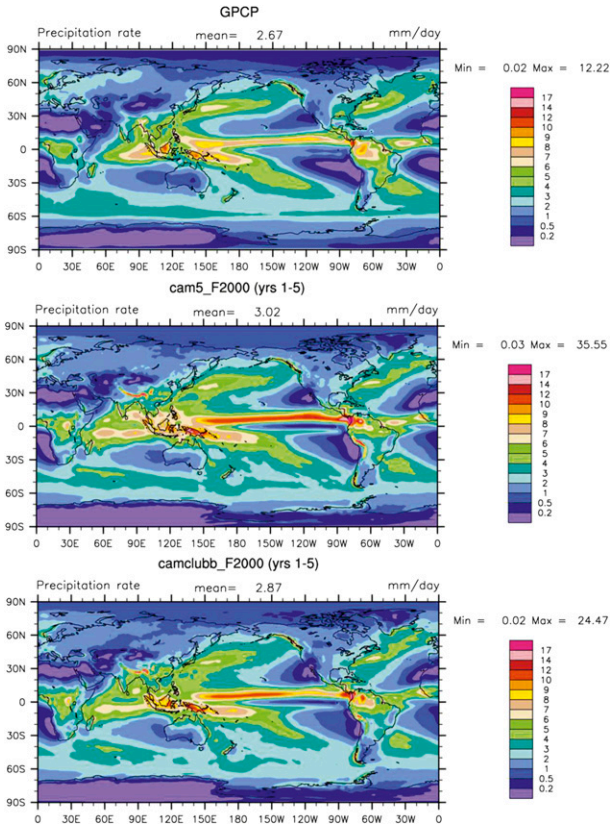

FIG. 7. As in Fig. 1, but for total precipitation rate with GPCP serving as the observational analysis.

Near the coast, where marine Sc is prevalent, $\overline{w'^3}$ is near zero and vertically homogenous, which is indicative of a low vertical velocity skewness and a coupled stratocumulus boundary layer. Farther away from the coast, where trade wind cumulus is present, $\overline{w'^3}$ increases in positive magnitude and develops a bimodal vertical structure, which is representative of a decoupled boundary layer cloud structure that is often found in trade cumulus regimes. This decoupled behavior is also seen in the vertical structure of $\overline{w'\theta_v'}$ in the columns farther away from the coast.

Indeed, the transition from the stratocumulus to cumulus like structure is simulated rather gradually by CAM–CLUBB. This is in contrast to CAM5, which uses separate schemes to parameterize marine Sc and Cu. Here we refer the reader to Figs. 11a,c of Park and Bretherton (2009), which display the parameterization budgets for CAM5 for a similar cross section. Although cloud fraction and buoyancy production in the stratocumulus regions (i.e., close to the coast) are somewhat similar in CAM5 and CAM–CLUBB, once the shallow convective mass flux takes over farther off the coast in CAM5 the cloud fraction becomes unrealistically small and is associated with a shallow depth. This indicates possible discrepancies/biases in the CAM5 shallow convection scheme that may be contributing to the relatively poor Sc–Cu transition in this model. In fact, Bogenschutz et al. (2012) shows that CAM–CLUBB can represent trade cumulus clouds more realistically than CAM5 in the SCM framework.

While it appears that CAM–CLUBB can overall improve the general cloud structure and transition characteristics compared to CAM5, a new turbulence parameterization should also provide improved vertical structure for the mean state thermodynamic variables. Figure 14 displays the cross sections of temperature and water vapor along the South American cross section for both CAM5 and CAM–CLUBB. Here the European Centre for Medium-Range Weather Forecasts (ECMWF) Interim Re-Analysis (ERA-Interim) is used as reference. To help reduce uncertainties in the ERA-Interim we also examined the cross sections of other observational analysis such as the Japanese 25-year Reanalysis Project (JRA-25) and Atmospheric Infrared Sounder (AIRS), which produced similar vertical structures to ERA-Interim. In terms of potential temperature transition, while both CAM5 and CAM–CLUBB's boundary layers are too warm near the coast compared to ERA-Interim, the problem seems a bit worse for CAM5. This is not surprising given that CAM5 generally produces less cloud than CAM–CLUBB in this region. Moving farther offshore, the inversion strength and height for CAM–CLUBB generally agrees favorably with ERA-Interim. On the other hand, because of the lack of cloud amount in the trade cumulus regions, the inversion strength is generally poorly represented for CAM5.

The same analysis can be made for the transition of the water vapor mixing ratio for CAM5 and CAM–CLUBB when compared to ERA-Interim (middle row of Fig. 14). Here, however, we see that both CAM5 and CAM–CLUBB contain too much vapor in the trade cumulus portion of the transition, while CAM–CLUBB's inversion strength and height tend to compare better with ERA-Interim throughout the transition. The bottom row of Fig. 14 displays the averaged profiles across the entire transition for CAM5, CAM–CLUBB, ERA-Interim, JRA-25, and AIRS. All observational analysis agree well in the mixed layer and show that both model configurations are too warm and too moist. Above 850 hPa there is some disagreement between observational analysis, which is likely a result of the very coarse vertical resolution in JRA-25 and AIRS. In general, the quantitative aspects of CAM–CLUBB in simulating inversion height and strength agree better with analysis displayed here.

We can further investigate differences between simulated temperature and moisture profiles by segregating

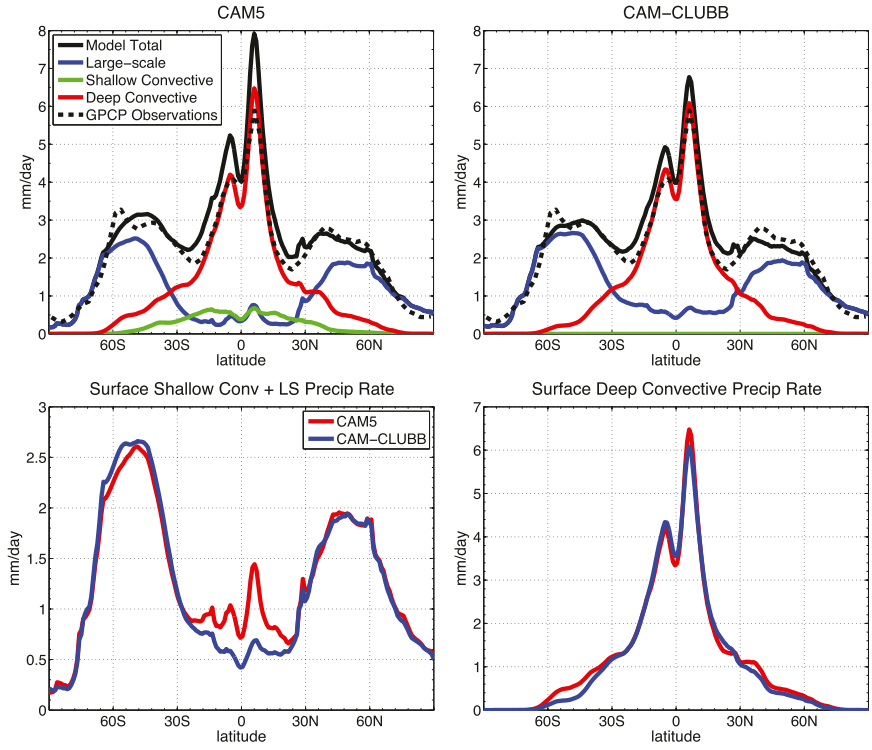

FIG. 8. (top) Zonal averages of surface precipitation rates from various parameterizations for CAM5 and CAM–CLUBB over the 5-yr simulation. (bottom left) The large-scale plus shallow convective precipitation rates and (bottom right) surface deep convective precipitation rate.

columns based on lower-tropospheric stability (LTS) and large-scale vertical velocity (ω) conditional sampling (Medeiros and Stevens 2011). Here we chose three regimes: stratocumulus, transitional cloud, and trade wind cumulus. We only consider oceanic points between 35°S and 35°N and the sampling criteria for these three cloud conditions can be found in Table 4. Although not shown here, we have verified that the distribution frequencies for these three cloud regimes are similar between CAM5 and CAM–CLUBB.

For the grid columns characterized by stratocumulus conditions, CAM–CLUBB tends to match analysis and observational guidance with more fidelity than CAM5 for both temperature and moisture (Fig. 15). This is true below 950 hPa where CAM5 is too warm and at inversion levels where CAM–CLUBB simulates a sharper inversion which agrees well with analysis/observations. For the grid columns identified as transitional or trade wind cumulus clouds CAM–CLUBB tends to agree better with analysis/observations in the subcloud mixed layer, where CAM–CLUBB is colder than CAM5 and above 800 hPa. However, CAM–CLUBB generally tends to be too cold in the layers occupied by clouds, which is likely indicative of cloud biases. Indeed, Fig. 12 indicates that in many transitional cloud regions CAM–CLUBB tends to predict too much liquid water compared to C3M observations, which can lead to a sharper inversion than seen in observations/analysis.

Finally, we examine differences in cloud-top height and amount in CAM5 and CAM–CLUBB. Figure 16

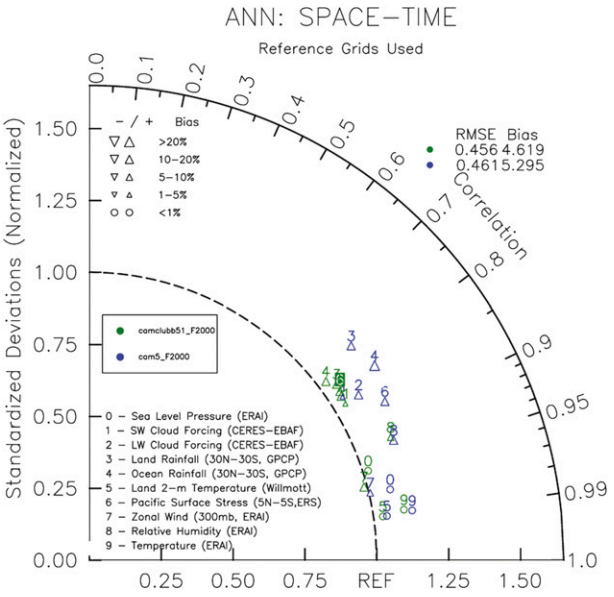

FIG. 9. Taylor diagram comparing scoring metrics of CAM5 (blue) and CAM–CLUBB (green) for the 5-yr simulation.

TABLE 3. Globally averaged value summary for CAM5, CAM–CLUBB, and observations.

Variable	Obs source	Units	CAM5	CAM–CLUBB	Obs
TOA imbalance	CERES-EBAF	$W m^{-2}$	4.6	3.3	1.0
TOA net solar flux	CERES-EBAF	$W m^{-2}$	242.3	242.4	240.6
TOA net longwave flux	CERES-EBAF	$W m^{-2}$	237.8	239.1	239.6
TOA LWCF	CERES-EBAF	$W m^{-2}$	22.5	21.8	26.5
TOA SWCF	CERES-EBAF	$W m^{-2}$	−48.8	−48.9	−47.1
Liquid water path	MODIS	$g m^{-2}$	43.2	42.8	112.62

displays one-dimensional histograms generated by the COSP simulator over the last 2 yr of simulation (Kay et al. 2012). Here we select the Multiangle Imaging SpectroRadiometer (MISR) simulator since the MISR satellite has been shown to be the best in detecting low-level cloud. Four regional histograms are displayed: global, Northern Hemisphere (NH) Pacific stratus region (15°–35°N, 150°–120°W), Southern Hemisphere (SH) Pacific stratus region (30°–5°S, 110°–80°W), and the Southern Ocean (oceanic points between 90° and 50°S). For cloud optical depths $\tau < 3.6$, there are large intersatellite differences for cloud fraction and this relates to differences in detection and treatment of cloud edges and therefore comparison of model versus observations at these low optical depths is not warranted (Kay et al. 2012).

In terms of the low cloud structure, CAM–CLUBB generally predicts thicker clouds that are in better agreement with MISR. This was also the finding for the trade cumulus cloud displayed in Figs. 11 and 12. However, the thicker clouds simulated by CAM–CLUBB appears to be at the expense of τ relationships with cloud amount, where CAM–CLUBB's cloud fraction tends to peak at optical depths that are slightly too high. This problem is especially evident in the NH Pacific stratus region, where CAM–CLUBB's SWCF is too strong for offshore stratocumulus. This problem is not apparent in the Southern Ocean, where CAM–CLUBB has better cloud fraction and τ relationship; however, CAM–CLUBB also tends to produce too much cloud amount in the lower troposphere. It should be noted that CAM–CLUBB is largely responsible for all heat and moisture tendencies in the storm track regions, whereas the tendencies provided from CAM5 are contributed from both the PBL and shallow convection schemes.

c. Sensitivity to vertical resolution

This section will focus on analysis of CAM5 and CAM–CLUBB sensitivity to changes in vertical resolution. Bogenschutz et al. (2012) found that CAM–CLUBB was more robust to changes in the vertical resolution than CAM5 in the single-column framework for GCSS idealized cases. Here we test this robustness in global climate simulations. Parameterizations that are less sensitive to the vertical resolution means that the model has to undergo less tuning when the aspect ratio of the grid is changed and it also gives us more faith that physics packages are giving the right answer for the right reason.

In this preliminary test we focus on sensitivity of CAM5 and CAM–CLUBB to differences in the vertical resolution. The standard configuration of CAM5 and CAM–CLUBB includes 30 vertical levels and it is expected in the coming years that the standard configuration will be nearly double that; therefore, we test experimental configurations with 60 vertical levels (CAM5-60 and CAM–CLUBB-60). The experimental grid takes the 30-layer grid and divides each level in half; therefore, we do not favor one particular layer of the atmosphere with our new grid. We run both CAM5-60 and CAM–CLUBB-60 at 1° for 2 yr. The only difference between the reference simulations and the higher vertical resolution simulations is the change of the vertical grid. The host model time step is kept the same as our

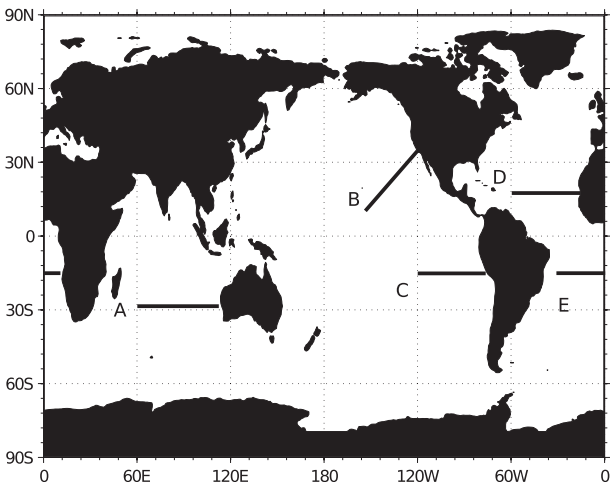

FIG. 10. Location of cross sections used for Sc–Cu transition analysis. Solid lines denote locations of cross sections. Location A refers to the Australia region, location B refers to the California region, location C refers to the South America region, location D refers to the North Africa region, and location E refers to the South Africa region.

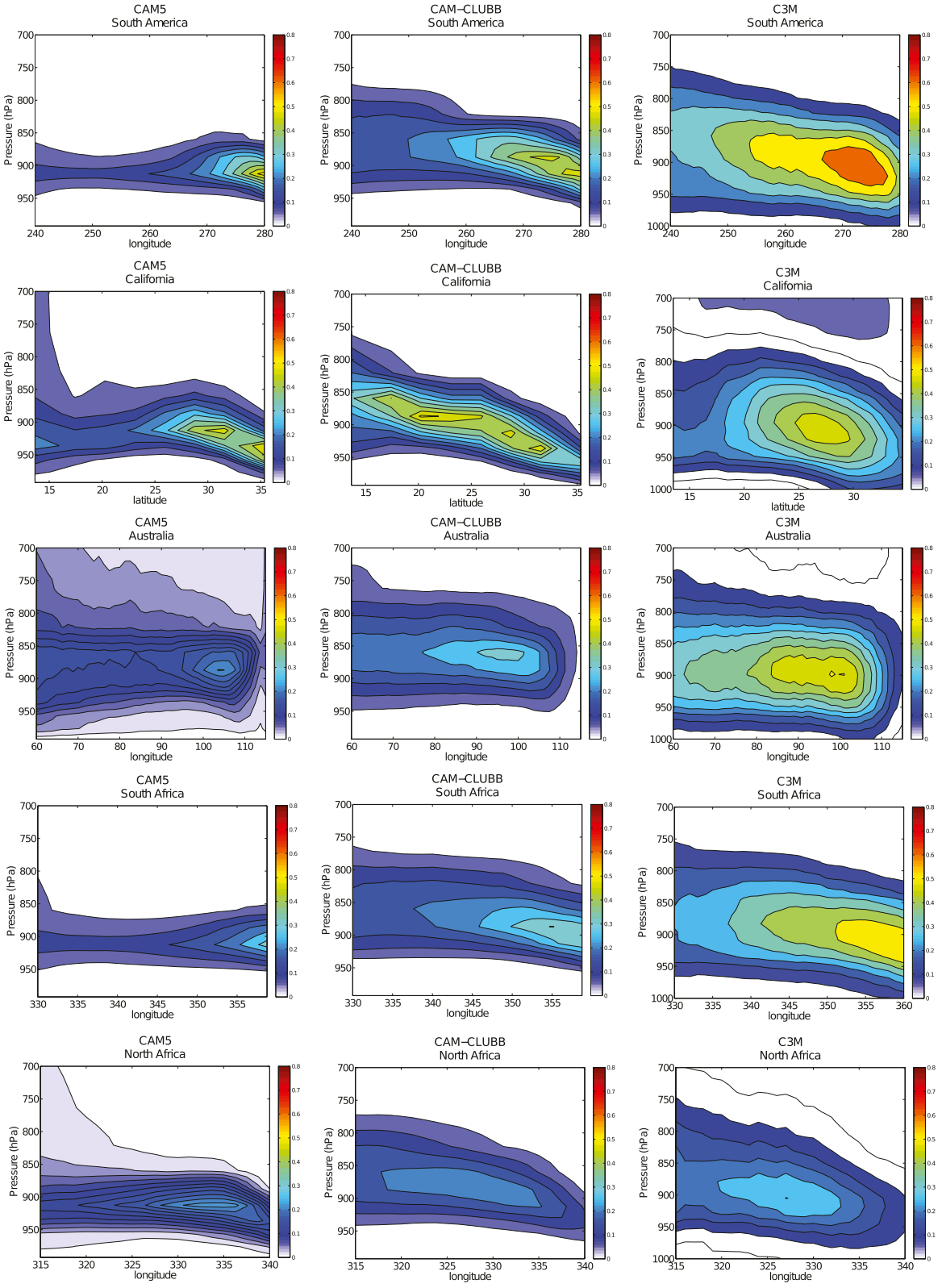

FIG. 11. Cross sections of cloud fraction from five locations for (left) CAM5, (center) CAM–CLUBB, and (right) C3M. Refer to the lines in Fig. 10 for the locations of the cross sections.

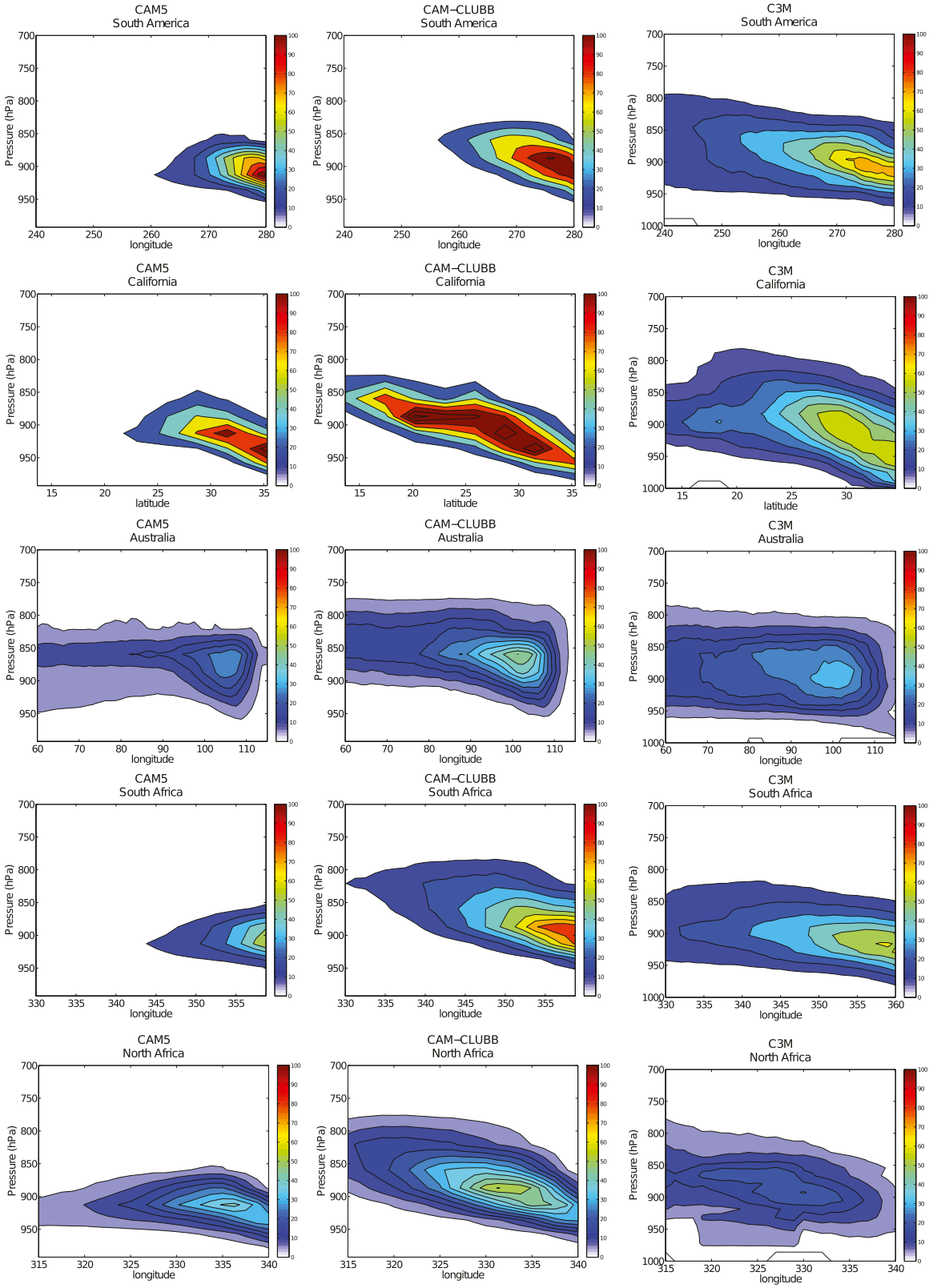

FIG. 12. As in Fig. 11, but for cloud liquid water mixing ratio (mg kg^{-1}).

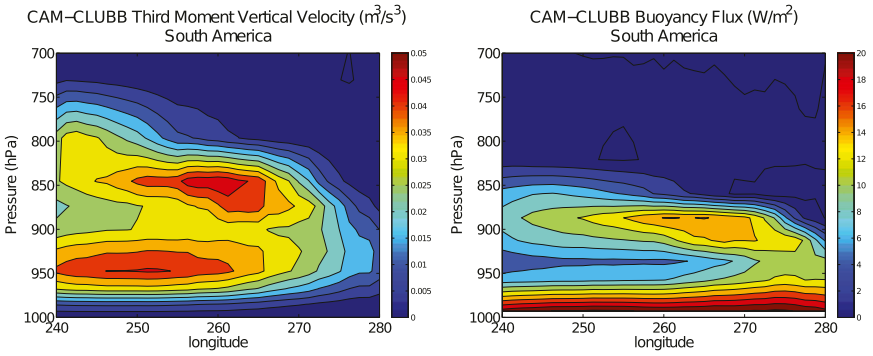

FIG. 13. Cross section of $\overline{w'^3}$ and $\overline{w'\theta_v'}$ as simulated by CAM–CLUBB for the South America cross section as denoted by line C in Fig. 10.

control simulations, although we have done short experiments with a smaller time step and the results were robust when compared to those shown in this paper.

Figure 17 displays the biases in simulated low cloud amount (top) and SWCF (bottom) for CAM5-60 (left) and CAM–CLUBB-60 (right). For comparison with biases in the operational (30 levels) configuration, refer to Fig. 2 for low-level cloud amount and Fig. 4 for SWCF. While one would expect boundary layer clouds to be simulated with better fidelity at 60 levels, it is clear that CAM5-60 suffers from a depletion of low-level clouds that is centered in the stratocumulus regions. It should be kept in mind that CAM5 already suffers from lack of low cloud in these regions in the standard configuration. Additional sensitivities for CAM5-60 are found in the trade wind cumulus regions. CAM–CLUBB-60, on the other hand, improves the representation of the Sc–Cu transition regions and trade cumulus regions compared to the standard 30-level configuration.

The story is a bit different when we examine the changes in SWCF for the two CAM configurations, where both CAM5-60 and CAM–CLUBB-60 degrade in the stratocumulus regions. However, CAM5-60 is relatively more sensitive to changes in SWCF over the entire global ocean. While CAM–CLUBB-60 is fairly robust globally in terms of SWCF, the degradation in the stratocumulus regions (mainly California and South America) is troubling and counterintuitive. However, it is important to note that other CAM parameterizations (i.e., microphysics, radiation, and deep convection) could be sensitive to changes in vertical grid spacing and could be contributing to the relatively poor SWCF representation in the Sc regions for CAM5-60 and CAM–CLUBB-60. However, the robustness in low cloud amount for CAM–CLUBB-60 suggests that perhaps it is not the CLUBB parameterization that is largely responsible for the differences in SWCF for CAM–CLUBB-60. Elucidating individual parameterization sensitivity in CAM5 (and other GCMs, in general) remains as challenging and important future work.

5. Summary and discussion

This paper presents global climate simulations of CAM coupled with a relatively new type of parameterization for use in GCMs, known as CLUBB. CLUBB is a higher-order turbulence closure that is centered around an assumed double-Gaussian trivariate probability density function. The novel aspect of CLUBB, compared to conventional GCM parameterizations, is that it is a unified parameterization of the PBL, shallow convection, and cloud macrophysics, meaning it calculates tendencies of these processes using only one equation set. This is very physically attractive compared to CAM5, which uses separate parameterizations for these processes, because it avoids any potential inconsistencies or undesired interactions that may arise from having separate schemes. In addition, CLUBB drives a single microphysics scheme (MG) for both shallow convection and stratiform cloud, whereas the shallow convection scheme in CAM5 has its own single-moment treatment of microphysics. Therefore CAM–CLUBB should allow for a more unified treatment of microphysics and cloud–aerosol interactions.

Results from 5-yr simulations at 1° horizontal resolution and 30 vertical levels of CAM–CLUBB and CAM5 are compared in this paper. Kay et al. (2012) find that although CAM5 greatly improves cloud representation of all types compared to CAM4, CAM5 still suffers from rather poor stratocumulus to cumulus transitions that are typically found in the subtropical oceans. Here we show that CAM–CLUBB can improve these transition areas as annually averaged cloud amounts and SWCF

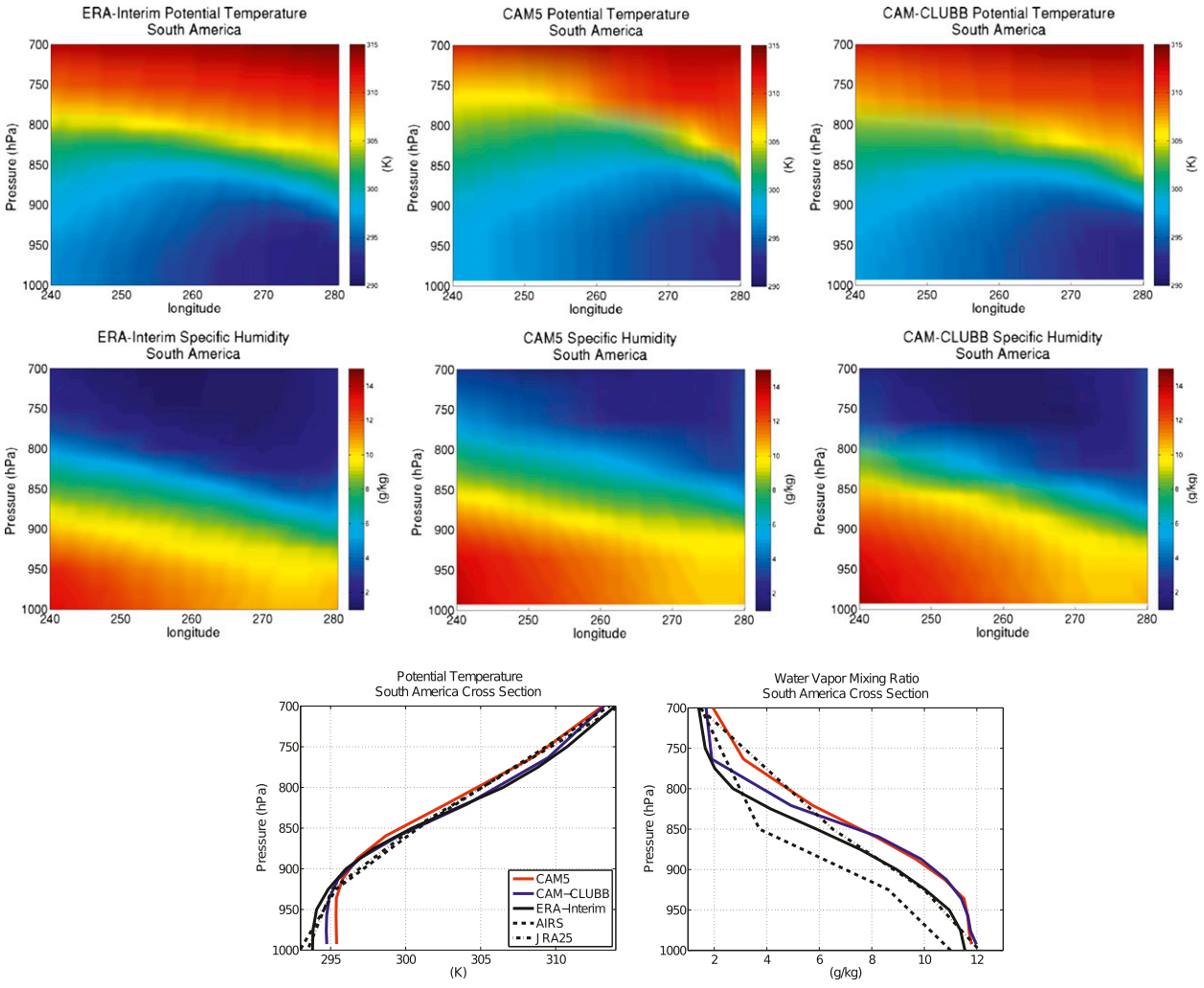

FIG. 14. (top) Potential temperature and (middle) water vapor mixing ratio cross sections for the South America region as denoted by line C in Fig. 10. (bottom) The averaged temperature and moisture profiles for both model and observations/analysis across the entire cross section.

show a more gradual transition of this particular regime. In addition, we show that CAM–CLUBB improves the representation of SWCF in the storm-track regions as well as over continental deep convective areas. CAM–CLUBB is also able to improve precipitation skill scores along the maritime deep convective regions, and this improvement seems to stem from smaller precipitation rates in shallow convection regimes in CAM–CLUBB than in CAM5. In general, CAM–CLUBB improves many persistent CAM5 biases while retaining skill scores of the general base state climate.

An analysis of the stratocumulus to cumulus transition is performed in five subtropical regions for CAM5 and CAM–CLUBB compared to C3M. For all regions we show CAM–CLUBB can more realistically represent these transitions through analysis of cross sections of cloud amount and cloud mass. While CAM5 abruptly transitions to cumulus, it also fails to capture the rising of cloud-top height across progressively warmer SSTs seen in C3M. CAM–CLUBB has a more gradual transition that improves over CAM5. While both CAM5 and

TABLE 4. Sampling criteria used to segregate stratocumulus, transitional clouds, and trade wind cumulus based on that of Medeiros and Stevens (2011).

Regime	LTS (K)	$\omega_{500\text{hPa}}$ and $\omega_{700\text{hPa}}$ (hPa day^{-1})
Stratocumulus	LTS $\geq$ 18.5	>10.0
Transitional cloud	18.5 > LTS $\geq$ 15.4	>10.0
Trade wind cumulus	15.4 > LTS $\geq$ 11.3	>10.0

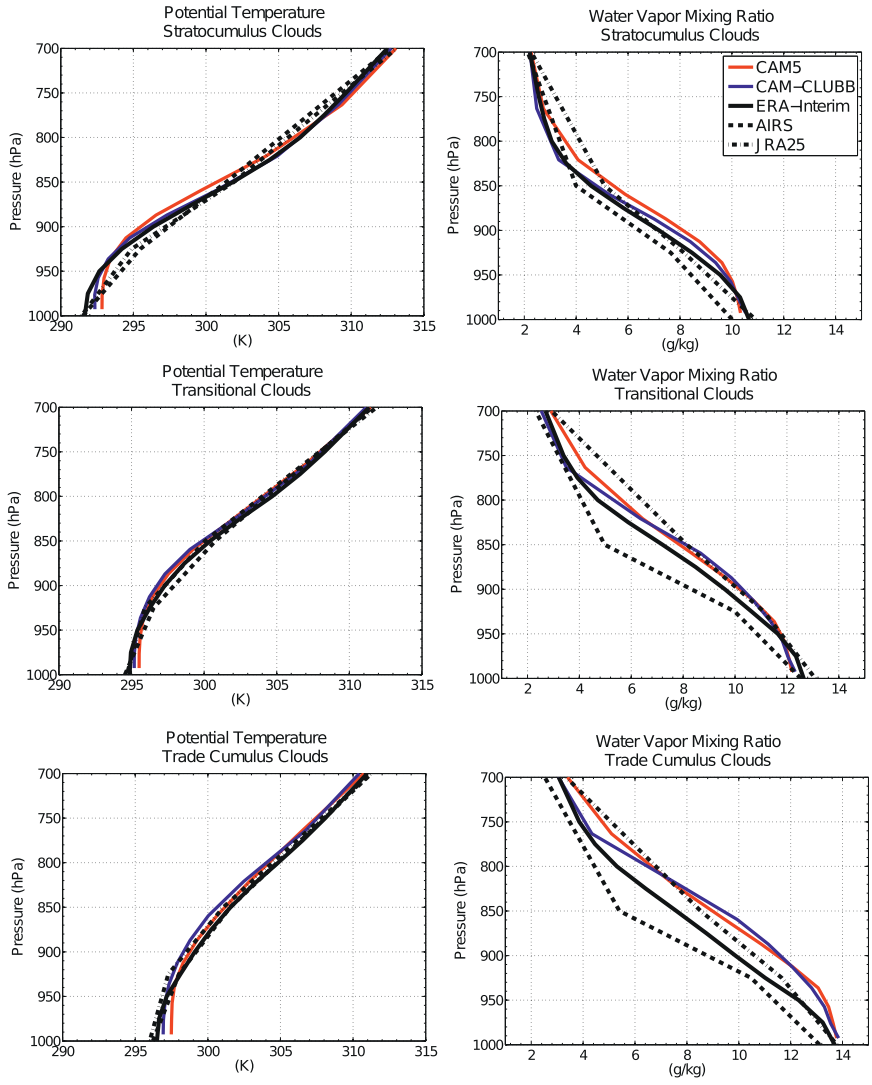

FIG. 15. (left) Potential temperature and (right) water vapor mixing ratio profiles for (top) stratocumulus clouds, (middle) transitional clouds, and (bottom) trade wind cumulus clouds. Refer to Table 4 for sampling rules.

CAM–CLUBB underpredict LWP in trade cumulus regions, CAM–CLUBB is closer to C3M. The more realistic transition in CAM–CLUBB appears to be the result of a smooth transition in the turbulence properties of the scheme, which is unified between stratocumulus and cumulus clouds. CAM5, on the other hand, uses separate schemes for these two different cloud types. The result is an abrupt transition to a cumulus like cloud type once the shallow convection mass flux scheme activates. Part of the improvement is also a result of the better fidelity of CAM–CLUBB to represent trade cumulus clouds compared to the CAM5 shallow convection scheme, which is in agreement with the SCM study of Bogenschutz et al. (2012). In addition, we show that CAM–CLUBB can represent the thermodynamics structure in these regimes with fidelity, while improving the relationships between cloud-top height and cloud amount relationships.

Through this analysis we show that CAM–CLUBB simulates quantitatively different boundary layer clouds compared to CAM5. Namely, these clouds are thicker than those simulated by CAM5 and more realistic when compared to C3M and MISR satellite observations. CAM–CLUBB trade cumulus and transitional clouds also appear to contain more liquid water compared to CAM5 clouds. These results could have significant implications for several reasons. First, these transitional and trade cumulus regions cover a much larger portion

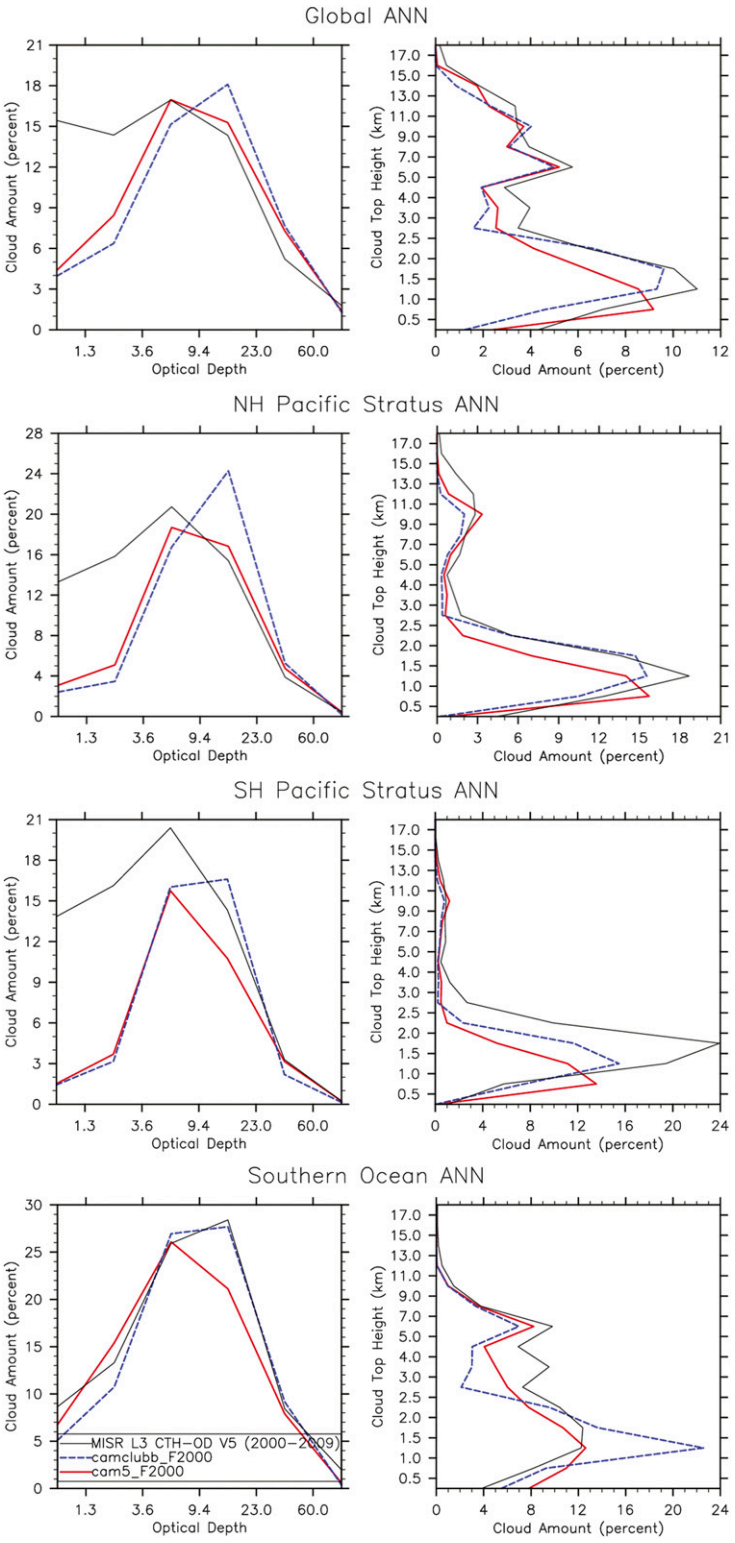

FIG. 16. Cloud amount as a function of (left) cloud-top height and (right) cloud-top pressure for CAM5 (red curve) and CAM–CLUBB (blue curve) as simulated by the MISR simulator and compared to MISR satellite retrievals. Curves shown here represent global averages over the last 2 yr of the 5-yr simulation. Refer to text for description of the boundaries for the four regions sampled.

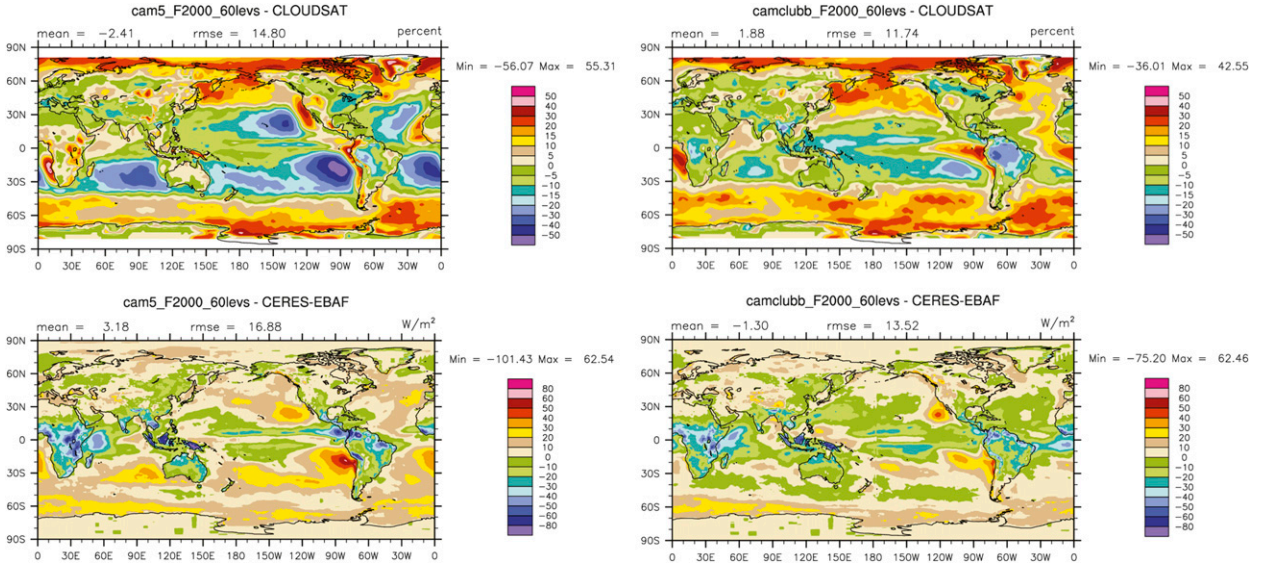

FIG. 17. The 2-yr annual average biases for (top) low cloud amount and (bottom) SWCF for (left) CAM5-60 and (right) CAM–CLUBB-60 compared to observations [*CloudSat* in (top) and CERES EBAF in (bottom)]. All difference plots represent the 60-level configuration minus the observation. For comparison with the standard (30 level) configuration biases, refer to Fig. 2 for (top) and Fig. 4 for (bottom).

of the tropical and subtropical ocean than do stratocumulus and this could have important implications for climate sensitivity experiments between these two configurations of CAM. Second, transitional and cumulus clouds for CAM–CLUBB contain interactive aerosols since CLUBB is coupled with the MG microphysics scheme. Therefore, all boundary layer clouds are subject to aerosol indirect effects in CAM–CLUBB and it will be interesting to compare aerosol indirect effects in these two versions of CAM in future work.

Section 4c of this paper also focused on sensitivities of CAM5 and CAM–CLUBB to vertical resolution with short duration simulations. Both configurations of CAM were run at 1° horizontal resolution with 60 vertical levels and we showed that CAM–CLUBB was more robust to the change in vertical resolution in terms of boundary layer cloud representation. This is in agreement with the SCM study of Bogenschutz et al. (2012). Whereas one would expect boundary cloud representation to improve as the vertical grid becomes more fine, CAM5 suffers from a significant loss of maritime stratocumulus clouds. This suggests some sensitivities of CAM5 physics packages to vertical resolution, which is not desirable. While CAM–CLUBB also suffers a loss of low stratiform cloud when increasing vertical resolution, it is less than CAM5 and the loss could be a result of interactions with other physics packages, which may not be optimized for high vertical resolution.

These are encouraging results as it is ideal to have physics in GCMs that are insensitive to changes in the vertical resolution as it points to the fact that the physics are scale insensitive, which is not only physically desirable in giving us more confidence that our parameterizations are giving us the right answers for the right reasons and but also because the GCM will not need significant retuning when running at different configurations.

The improved results found in this paper for CAM–CLUBB, which includes better Sc–Cu transition and more robust results to changes in vertical grid spacing, can be attributed to the more unified nature of the CLUBB parameterization compared to CAM5 physics and better fidelity in simulating trade wind cumulus clouds. Medeiros et al. (2012) found that, while CAM5 can represent marine stratocumulus better than CAM4, often times the overactivation of the shallow convective scheme can hinder stratocumulus forecasts. Indeed, Bogenschutz et al. (2012) found similar results in a SCM study; the activation of the shallow convective scheme can deteriorate the diurnal cycle of marine Sc in high vertical resolution simulations. In addition, Bogenschutz et al. (2012) found that CAM5 cannot realistically represent a stationary case of Cu under Sc because the shallow convective scheme dominates. CAM–CLUBB avoids this inconsistency by unifying PBL and shallow convective processes into one parameterization that uses one equation set. This allows for turbulent processes to evolve gradually across cloud transition regions.

However, some current weaknesses of CAM–CLUBB include a degradation of coastal California Sc and

reduced skill scores for LWCF. The latter problem is likely linked to a lack of a cloud-top radiative cooling parameterization in CLUBB for coarse vertical grid sizes, such as that presented in Bretherton and Park (2009). The former weakness is because unified parameterizations are inherently harder to tune since the same equation set is responsible for simulating a wide range of cloud conditions. Finally, while this paper mostly focused on representation of subtropical and tropical clouds, future work should address representation of polar and mixed-phase clouds in CAM–CLUBB. Initial assessment suggests that CAM–CLUBB has nearly identical representation of these types of clouds compared to CAM5, which is generally considered to be inferior when compared to observations, despite nearly completely different cloud forming physics.

The preliminary results of CAM–CLUBB show promise toward the use of this unique and unified parameterization in GCMs and opens many possible avenues for future development. For instance, integrating over CLUBB's SGS PDF, one can generate subcolumns that can be used for consideration of microphysics calculations to avoid cloud overlap assumptions (Pincus et al. 2006). In addition, for a better physical coupling to the MG microphysics scheme, it is possible to substep CLUBB and microphysics together at the CLUBB time step instead of tendencies from these two schemes being applied in a completely process split manner, as is currently done. Since CLUBB is a unified parameterization this would mean that boundary clouds and microphysics evolve/integrate together, which is somewhat analogous to how a cloud-resolving model works. Finally, CAM–CLUBB could in principle be used to simulate deep convective processes. This would represent a truly unified cloud, convection, and turbulence scheme of all cloud types that would drive only one microphysics scheme (MG). In fact, CAM–CLUBB has already been run in such a configuration for short simulations and the initial results are encouraging. However, this fully unified configuration of CAM–CLUBB will remain as future work.

The results presented in this paper also lead to several scientific experiments that can and will be explored with CAM–CLUBB. For instance, since CAM–CLUBB provides a more consistent treatment of cloud–aerosol interactions compared to CAM5, it should follow that aerosol indirect experiments should be conducted with CAM–CLUBB. The hope is that aerosol processes will be more realistically simulated with this version of CAM. In addition, many other experiments such as the comparison of cloud feedbacks and climate sensitivity between CAM–CLUBB and CAM5 should also be explored since these two model configurations have different representations of oceanic boundary layer clouds. Finally, while initial 25-yr coupled simulations have been performed with the same version of CAM–CLUBB presented in this paper with a stable climate, it will be important to note how CAM–CLUBB performs in the fully coupled Community Earth System Model (CESM) for longer-term climate simulations.

Acknowledgments. Peter A. Bogenschutz is supported by National Science Foundation Grant 0968657. V. Larson and D. Schanen gratefully acknowledge financial support under Grant 0968640 from the National Science Foundation and Grant DE-SC0006927 from the SciDAC program of the U.S. Department of Energy. The authors are grateful to Lin Su and Chin-Chieh (Jack) Chen for reading and suggesting improvements to this manuscript.

APPENDIX A

Description of Tuning Parameters Used in CAM–CLUBB

The CLUBB parameterization includes many tunable parameters that can be modified. However, here we only discuss the two parameters that we have modified for the purposes of CAM-CLUBB. In addition, we have tuned several CAM5 variables and their justifications are discussed here as well.

a. C11b

This parameter is described in Golaz et al. (2007) and was added to the CLUBB code to better distinguish between Sc and Cu regimes in SCM experiments. This term appears in the important $\overline{w'^3}$ predictive equation in the buoyancy and gradient production terms. Larger values help to promote more Sc because of generally lower $\overline{w'^3}$ values globally. Our initial impression with the default value (0.3) is that globally averaged low-level cloud amounts are too low. We find that a value of C11b = 0.65 is a good compromise in attaining reasonable low-level cloud while also allowing for cumulus layers to be sufficiently skewed.

b. Skw_denom_coef

This clipping parameter was recently introduced to CLUBB help prevent the vertical velocity skewness from becoming too large in the morning hours of marine stratocumulus, should $\overline{w'^3}$ become sufficiently larger than $\overline{w'^2}$. The default value is 8.0. However, we find that this default value leads to trade wind cumulus layers that

are too reflective and too Gaussian. Thus, we set this parameter to 0.0. Note that this is the same value that was essentially used in Bogenschutz et al. (2012) before this parameter was introduced.

c. Cloud water variance

As discussed in section 2, we now feed MG microphysics a variable cloud water variance for consideration in the computation of the relative cloud water variance γ. In CAM5, γ is set to a constant 2.0. Although we consider the inclusion of a variable γ to be a physics upgrade, we tuned the constrained γ values. In CAM–CLUBB we constrain γ in the range of $0.001 < \gamma < 1.0$. Results are generally insensitive to the lower bound, but reducing the maximum γ from 2.0 was required to achieve reasonable SWCF magnitudes. Our reduced 1.0 maximum, however, was the γ value selected in the initial implementation of MG in Morrison and Gettelman (2008).

d. Aerosol scavenging efficiency

In CAM5 stratiform and convective cloud have different scavenging rules. Because CAM–CLUBB produces much different trade wind cumulus clouds than CAM5 and because CAM–CLUBB cumulus clouds are now linked with interactive aerosols, we found it necessary to reduce the scavenging efficiency for stratiform cloud in CAM–CLUBB to achieve the same globally averaged aerosol optical depth (AOD) as in CAM5. The default value is 1.0 in CAM5; in CAM–CLUBB we reduce this to 0.6.

e. Dust mobilization

To achieve similar dust optical depth for CAM–CLUBB and CAM5, a tunable parameter in the Community Land Model (CLM; Bonan et al. 2011) needs to be modified. Here the constant flx_mss_fdg_fct is reduced from 1.2×10^{-3} to 5.0×10^{-4} (no units). In the future it will be judicious to examine differences in the clear convective boundary layer in global simulations over Africa between CAM5 and CAM–CLUBB that likely leads to this needed tuning modification.

f. Ice SGS vertical velocity

Since CLUBB does not currently contain a cloud-top radiative cooling parameterization, similar to one documented in Bretherton and Park (2009), upper-tropospheric turbulence in the midlatitudes is often underestimated which leads to a lack of ice nucleation. As a temporary fix, we increase the minimum value of the ice SGS vertical velocity. We increase it by an order of magnitude if the ice SGS vertical velocity is less than $0.04\,\mathrm{m\,s^{-1}}$. This only has an effect in the upper troposphere in the storm tracks, as high cloud in the ITCZ is strongly dominated by the detrainment of liquid water from the deep convection scheme.

APPENDIX B

CLUBB Governing Equations

Here we describe the CLUBB predictive equations for reference. CLUBB predicts the grid-average horizontal winds $(\overline{u}, \overline{v})$, liquid water potential temperature $\overline{\theta_l}$, and total water mixing ratio $\overline{q_t}$. In addition, CLUBB predicts eight second-order moments and one-third-order moment $\overline{w'^3}$. The governing equations are as follows:

$$\frac{\partial \overline{u}}{\partial t} = -\overline{w}\frac{\partial \overline{u}}{\partial z} - f(\overline{v}_g - \overline{v}) - \frac{\partial}{\partial z}\overline{u'w'}, \tag{B1}$$

$$\frac{\partial \overline{v}}{\partial t} = -\overline{w}\frac{\partial \overline{v}}{\partial z} - f(u_g - \overline{u}) - \frac{\partial}{\partial z}\overline{v'w'}, \tag{B2}$$

$$\frac{\partial \overline{q_t}}{\partial t} = -\overline{w}\frac{\partial \overline{q_t}}{\partial z} - \frac{\partial}{\partial z}(\overline{w'q_t'}) + \left.\frac{\partial \overline{q_t}}{\partial t}\right|_{\mathrm{ls}}, \tag{B3}$$

$$\frac{\partial \overline{\theta_l}}{\partial t} = -\overline{w}\frac{\partial \overline{\theta_l}}{\partial z} - \frac{\partial}{\partial z}(\overline{w'\theta_l'}) + \overline{R} + \left.\frac{\partial \overline{\theta_l}}{\partial t}\right|_{\mathrm{ls}}, \tag{B4}$$

$$\frac{\partial \overline{w'^2}}{\partial t} = -\overline{w}\frac{\partial \overline{w'^2}}{\partial z} - \frac{\partial \overline{w'^3}}{\partial z} - 2\overline{w'^2}\frac{\partial \overline{w}}{\partial z} + \frac{2g}{\theta_0}\overline{w'\theta_v'} - C_5\left(-2\overline{w'^2}\frac{\partial \overline{w}}{\partial z} + \frac{2g}{\theta_0}\overline{w'\theta_v'}\right) + \frac{2}{3}C_5\left(\frac{g}{\theta_0}\overline{w'\theta_v'} - \overline{u'w'}\frac{\partial \overline{u}}{\partial z} - \overline{u'w'}\frac{\partial \overline{v}}{\partial z}\right) + \frac{C_1}{\tau}\overline{w'^2} + \nu_1\nabla_z^2\overline{w'^2}, \tag{B5}$$

$$\frac{\partial \overline{q_t'^2}}{\partial t} = -\overline{w}\frac{\partial \overline{q_t'^2}}{\partial z} - \frac{\partial \overline{w'q_t'^2}}{\partial z} - 2\overline{w'q_t'}\frac{\partial \overline{q_t}}{\partial z} - \frac{C_2}{\tau}\overline{q_t'^2} + \nu_2\nabla_z^2\overline{q_t'^2}, \tag{B6}$$

$$\frac{\partial \overline{\theta_l'^2}}{\partial t} = -\overline{w}\frac{\partial \overline{\theta_l'^2}}{\partial z} - \frac{\partial \overline{w'\theta_l'^2}}{\partial z} - 2\overline{w'\theta_l'}\frac{\partial \overline{\theta_l}}{\partial z} - \frac{C_2}{\tau}\overline{\theta_l'^2} + \nu_2\nabla_z^2\overline{\theta_l'^2}, \tag{B7}$$

$$\frac{\partial \overline{q_t' \theta_l'}}{\partial t} = -\overline{w}\frac{\partial \overline{q_t' \theta_l'}}{\partial z} - \frac{\partial \overline{w' q_t' \theta_l'}}{\partial z} - \overline{w' \theta_l'}\frac{\partial \overline{q_t}}{\partial z} - \overline{w' q_t'}\frac{\partial \overline{\theta_l}}{\partial z} - \frac{C_2}{\tau}\overline{q_t' \theta_l'} + \nu_2 \nabla_z^2 \overline{q_t' \theta_l'}, \tag{B8}$$

$$\frac{\partial \overline{w' q_t'}}{\partial t} = -\overline{w}\frac{\partial \overline{w' q_t'}}{\partial z} - \frac{\partial \overline{w'^2 q_t'}}{\partial z} - \overline{w'^2}\frac{\partial \overline{q_t}}{\partial z} - \overline{w' q_t'}\frac{\partial \overline{w}}{\partial z} + \frac{g}{\theta_0}\overline{q_t' \theta_v'} - \frac{C_6}{\tau}\overline{w' q_t'} + C_7\left(-\overline{w' q_t'}\frac{\partial \overline{w}}{\partial z} + \frac{g}{\theta_0}\overline{q_t' \theta_v'}\right) + \nu_6 \nabla_z^2 \overline{w' q_t'}, \tag{B9}$$

$$\frac{\partial \overline{w' \theta_l'}}{\partial t} = -\overline{w}\frac{\partial \overline{w' \theta_l'}}{\partial z} - \frac{\partial \overline{w'^2 \theta_l'}}{\partial z} - \overline{w'^2}\frac{\partial \overline{\theta_l}}{\partial z} - \overline{w' \theta_l'}\frac{\partial \overline{w}}{\partial z} + \frac{g}{\theta_0}\overline{\theta_l' \theta_v'} - \frac{C_6}{\tau}\overline{w' \theta_l'} + C_7\left(-\overline{w' \theta_l'}\frac{\partial \overline{w}}{\partial z} + \frac{g}{\theta_0}\overline{\theta_l' \theta_v'}\right) + \nu_6 \nabla_z^2 \overline{w' \theta_l'}, \tag{B10}$$

$$\frac{\partial \overline{w'^3}}{\partial t} = -\overline{w}\frac{\partial \overline{w'^3}}{\partial z} - \frac{\partial \overline{w'^4}}{\partial z} + 3\overline{w'^2}\frac{\partial \overline{w'^2}}{\partial z} - 3\overline{w'^3}\frac{\partial \overline{w}}{\partial z} + \frac{3g}{\theta_0}\overline{w'^2 \theta_v'} - \frac{C_8}{\tau}(C_{8b} S k_w^4 + 1)\overline{w'^3} - C_{11}\left(-3\overline{w'^3}\frac{\partial \overline{w}}{\partial z} + \frac{3g}{\theta_0}\overline{w'^2 \theta_v'}\right) + (K_w + \nu_8)\nabla_z^2 \overline{w'^3}, \tag{B11}$$

$$\frac{\partial \overline{u'^2}}{\partial t} = -\overline{w}\frac{\partial \overline{u'^2}}{\partial z} - \frac{\partial}{\partial z}\overline{w' u'^2} - (1 - C_5)2\overline{u' w'}\frac{\partial \overline{u}}{\partial z} - \frac{2}{3}C_{14}\frac{\overline{e}}{\tau} + \frac{2}{3}C_5\left(\frac{g}{\overline{\theta}_v}\overline{w' \theta_v'} - \overline{u' w'}\frac{\partial \overline{u}}{\partial z} - \overline{v' w'}\frac{\partial \overline{v}}{\partial z}\right) - \frac{C_4}{\tau}\left(\overline{u'^2} - \frac{2}{3}\overline{e}\right) + \frac{\partial}{\partial z}\left[(c_{K9} K_m + \nu_9)\frac{\partial}{\partial z}\overline{u'^2}\right], \quad \text{and} \tag{B12}$$

$$\frac{\partial \overline{v'^2}}{\partial t} = -\overline{w}\frac{\partial \overline{v'^2}}{\partial z} - \frac{\partial}{\partial z}\overline{w' v'^2} - (1 - C_5)2\overline{v' w'}\frac{\partial \overline{v}}{\partial z} - \frac{2}{3}C_{14}\frac{\overline{e}}{\tau} + \frac{2}{3}C_5\left(\frac{g}{\overline{\theta}_v}\overline{w' \theta_v'} - \overline{v' w'}\frac{\partial \overline{u}}{\partial z} - \overline{v' w'}\frac{\partial \overline{v}}{\partial z}\right) - \frac{C_4}{\tau}\left(\overline{v'^2} - \frac{2}{3}\overline{e}\right) + \frac{\partial}{\partial z}\left[(c_{K9} K_m + \nu_9)\frac{\partial}{\partial z}\overline{v'^2}\right], \tag{B13}$$

where $\overline{R}$ is the radiative heating rate; f is Coriolis parameter; u_g and v_g are the geostrophic winds; and $(\partial \overline{q_t}/\partial t)|_{\text{ls}}$ and $(\partial \overline{\theta_l}/\partial t)|_{\text{ls}}$ are large-scale moisture and temperature forcings, respectively. For a complete formulation of closure assumptions used for some of these terms please refer to Golaz et al. (2007) and Larson et al. (2002, 2012).

REFERENCES

Arakawa, A., 2004: The cumulus parameterization problem: Past, present, and future. *J. Climate,* **17,** 2494–2525.

Bogenschutz, P. A., A. Gettelman, H. Morrison, V. E. Larson, D. P. Schanen, N. R. Meyer, and C. Craig, 2012: Unified parameterization of the planetary boundary layer and shallow convection with a higher-order turbulence closure in the Community Atmosphere Model. *Geosci. Model Dev.,* **5,** 1407–1423.

Bonan, G. B., P. J. Lawrence, K. W. Oleson, S. Levis, M. Jung, M. Reichstein, D. M. Lawrence, and S. C. Swenson, 2011: Improving canopy processes in the Community Land Model version 4 (CLM4) using global flux fields empirically inferred from FLUXNET data. *J. Geophys. Res.,* **116,** G02014, doi:10.1029/2010JG001593.

Bougeault, P., 1981: Modeling the trade-wind cumulus boundary layer. Part II: A higher-order one-dimensional model. *J. Atmos. Sci.,* **38,** 2429–2439.

Bretherton, C. S., and S. Park, 2009: A new moist turbulence parameterization in the Community Atmosphere Model. *J. Climate,* **22,** 3422–3448.

Cheng, A., and K.-M. Xu, 2008: Simulation of boundary-layer cumulus and stratocumulus clouds using a cloud-resolving model with low and third-order turbulence closures. *J. Meteor. Soc. Japan,* **86,** 67–86.

——, and ——, 2011: Improved low-cloud simulation from a multiscale modeling framework with a third-order turbulence closure in its cloud resolving model component. *J. Geophys. Res.,* **115,** D14101, doi:10.1029/2010JD015362.

Gettelman, A., and Coauthors, 2010: Global simulations of ice nucleation and ice supersaturation with an improved cloud scheme in the Community Atmosphere Model. *J. Geophys. Res.,* **115,** D18216, doi:10.1029/2009JD013797.

Ghan, S. J., L. R. Leung, R. C. Easter, and H. Abdul-Razzak, 1997: Prediction of cloud droplet number in a general circulation model. *J. Geophys. Res.,* **102,** 21 777–21 794.

Golaz, J.-C., V. E. Larson, and W. R. Cotton, 2002: A PDF-based model for boundary layer clouds. Part I: Method and model description. *J. Atmos. Sci.,* **59,** 3540–3551.

——, S. Wang, J. D. Doyle, and J. M. Schmidt, 2005: COAMPS-LES: Model evaluation and analysis of second- and third-moment vertical velocity budgets. *Bound.-Layer Meteor.,* **116,** 487–517.

——, V. E. Larson, J. A. Hansen, D. P. Schanen, and B. M. Griffen, 2007: Elucidating model inadequacies in a cloud parameterization by use of an ensemble-based calibration framework. *Mon. Wea. Rev.,* **135,** 4077–4096.

Guo, H., J.-C. Golaz, L. J. Donner, V. E. Larson, D. P. Schanen, and B. M. Griffin, 2010: Multi-variate probability density functions with dynamics for cloud droplet activation in large-scale models: Single column tests. *Geosci. Model Dev.,* **3,** 475–486.

Iacono, M. J., J. S. Delamere, E. J. Mlawer, M. W. Shepard, S. A. Clough, and W. D. Collins, 2008: Radiative forcing by long-lived greenhouse gases: Calculations with the AER radiative transfer models. *J. Geophys. Res.,* **113,** D13103, doi:10.1029/2008JD009944.

Kato, S., S. Sun-Mack, W. F. Miller, F. G. Rose, Y. Chen, P. Minnis, and B. A. Wielicki, 2010: Relationships among cloud occurrence frequency, overlap, and effective thickness derived from CALIPSO and CloudSat merged cloud vertical profiles. *J. Geophys. Res.,* **115,** D00H28, doi:10.1029/2009JD012277.

Kay, J. E., and Coauthors, 2012: Exposing global cloud biases in the Community Atmosphere Model (CAM) using satellite

observations and their corresponding instrument simulators. *J. Climate,* **25,** 5190–5207.

Khairoutdinov, M. F., D. A. Randall, and C. Dermott, 2005: Simulations of the atmospheric general circulation using a cloud-resolving model as a superparameterization of physical processes. *J. Atmos. Sci.,* **62,** 2136–2154.

Lappen, C.-L., and D. A. Randall, 2001: Toward a unified parameterization of the boundary layer and moist convection. Part I: A new type of mass flux model. *J. Atmos. Sci.,* **58,** 2021–2035.

Larson, V. E., J.-C. Golaz, and W. R. Cotton, 2002: Small-scale and mesoscale variability in cloudy boundary layers: Joint probability density functions. *J. Atmos. Sci.,* **59,** 3519–3539.

——, D. P. Schanen, M. Wang, M. Ovchinnikov, and S. Ghan, 2012: PDF parameterization of boundary layer clouds in models with horizontal grid spacings from 2 to 16 km. *Mon. Wea. Rev.,* **140,** 285–306.

Liu, X., and Coauthors, 2012: Toward a minimal representation of aerosols in climate models: Description and evaluation in the Community Atmosphere Model CAM5. *Geosci. Model Dev.,* **5,** 709–739.

Medeiros, B., and B. Stevens, 2011: Revealing differences in GCM representations of low clouds. *Climate Dyn.,* **36,** 385–399.

——, D. L. Williamson, C. Hannay, and J. G. Olson, 2012: Southeast Pacific stratocumulus in the Community Atmosphere Model. *J. Climate,* **25,** 6175–6192.

Miura, H., H. Tomita, T. Nasuno, S. Iga, M. Satoh, and T. Matsuno, 2005: A climate sensitivity test using a global cloud resolving model under an aqua planet condition. *Geophys. Res. Lett.,* **32,** L19717, doi:10.1029/2005GL023672.

Moeng, C.-H., and D. A. Randall, 1984: Problems in simulation the stratocumulus-topped boundary layer with a third-order closure model. *J. Atmos. Sci.,* **41,** 1588–1600.

Morrison, H., and A. Gettelman, 2008: A new two-moment bulk stratiform cloud microphysics scheme in the Community Atmosphere Model, version 3 (CAM3). Part I: Description and numerical tests. *J. Climate,* **21,** 3642–3659.

Neale, R. B., J. H. Richter, and M. Jochum, 2008: The impact of convection on ENSO: From a delayed oscillator to a series of events. *J. Climate,* **21,** 5904–5924.

——, and Coauthors, 2010: Description of the NCAR Community Atmosphere Model (CAM 5.0). NCAR Tech. Note NCAR/TN-486+STR, 283 pp.

Park, S., and C. S. Bretherton, 2009: The University of Washington shallow convection and moist turbulence schemes and their impact on climate simulations with the Community Atmosphere Model. *J. Climate,* **22,** 3449–3469.

Pergaud, J., V. Masson, S. Malardel, and F. Couvreux, 2009: A parameterization of dry thermals and shallow cumuli for mesoscale numerical weather prediction. *Bound.-Layer Meteor.,* **132,** 83–106.

Pincus, R., R. Hemler, and S. Klein, 2006: Using stochastically generated subcolumns to represent cloud structure in a large-scale model. *Mon. Wea. Rev.,* **134,** 3644–3656.

Richter, J. H., and P. J. Rasch, 2008: Effects of convective momentum transport on the atmospheric circulation in the Community Atmosphere Model, version 3. *J. Climate,* **21,** 1487–1499.

Siebesma, A. P., P. M. M. Soares, and J. Teixeira, 2007: A combined eddy-diffusivity mass-flux approach for the convective boundary layer. *J. Atmos. Sci.,* **64,** 1230–1248.

Taylor, K. E., 2001: Summarizing multiple aspects of model performance in a single diagram. *J. Geophys. Res.,* **106,** 7183–7192.

Teixeira, J., and Coauthors, 2011: Tropical and subtropical cloud transitions in weather and climate prediction models: The GCSS/WGNE Pacific Cross-Section Intercomparison (GPCI). *J. Climate,* **24,** 5223–5256.

Tomita, H., H. Miura, S. Iga, T. Nasuno, and M. Satoh, 2005: A global cloud-resolving simulation: Preliminary results from an aqua planet experiment. *Geophys. Res. Lett.,* **32,** L08805, doi:10.1029/2005GL022459.

Zhang, G. J., and N. A. McFarlane, 1995: Sensitivity of climate simulations to the parameterization of cumulus convection in the Canadian Climate Centre General Circulation Model. *Atmos.–Ocean,* **33,** 407–446.